NASA SP-8038

N71-17525

NASA SPACE VEHICLE DESIGN CRITERIA (ENVIRONMENT)

METEOROID ENVIRONMENT MODEL-1970 [INTERPLANETARY AND PLANETARY]

October 1970

NATIONAL AERONAUTICS AND SPACE ADMINISTRATION

FOREWORD

NASA experience has indicated a need for uniform design criteria for space vehicles. Accordingly, criteria are being developed in the following areas of technology:

Environment
Structures
Guidance and Control
Chemical Propulsion

Individual components will be issued as separate monographs as soon as they are completed. A list of all previously issued monographs in this series can be found on the last page of this publication.

These monographs serve as guides to NASA design and mission planning. They are used to develop requirements for specific projects and also are cited as the applicable references in mission studies and in contracts for design and development of space vehicle systems.

This monograph was prepared by D. J. Kessler of the NASA Manned Spacecraft Center with the assistance of an ad hoc committee, chaired by C. T. D'Aiutolo, NASA Headquarters. The program coordinators were M. T. Charak of NASA Headquarters and S. A. Mills of the Goddard Space Flight Center. Participation and contribution of the following ad hoc committee members are hereby acknowledged:

A. J. Beck	Jet Propulsion Laboratory California Institute of Technology
B. G. Cour-Palais	NASA, Manned Spacecraft Center
J. Deerwester	NASA, Ames Research Center
T. N. Divine	Jet Propulsion Laboratory California Institute of Technology
J. S. Dohnanyi	Bellcomm
J. Howard	Jet Propulsion Laboratory California Institute of Technology
W. H. Kinard	NASA, Langley Research Center

R. J. Naumann NASA, Marshall Space Flight Center

C. R. Savin NASA, Ames Research Center

Comments concerning the technical content of these monographs will be welcomed by the National Aeronautics and Space Administration, Goddard Space Flight Center, Systems Reliability Directorate, Greenbelt, Md. 20771.

October 1970

For sale by the National Technical Information Service, Springfield, Virginia 22151 – Price $3.00

CONTENTS

METEOROID ENVIRONMENT MODEL - 1970 (INTERPLANETARY AND PLANETARY)

1. INTRODUCTION

Meteoroids are solid particles moving in space that are believed to originate from both cometary and asteroidal sources. Because of their velocity, density, and mass, meteoroids can cause damage to vehicles operating in space. The type and extent of the damage depend upon vehicle structural configuration and exposure time in space, as well as on the meteoroid characteristics. Meteoroid impact on a space vehicle can result in damage such as the puncture of a pressurized cabin, radiator, or propellant tank; the deterioration of windows, optical surfaces, and thermal balance coatings by cratering and spallation; or reduction of heat shield effectiveness. Other possible impact effects include damage to antenna systems, thruster nozzles, and electrical leads.

This monograph defines the meteoroid environment from 0.1 to 30.0 astronomical units (AU) outward from the sun in the mass range between 10^{-12} and 10^{2} grams. A detailed model of this environment is presented as number of particles per unit volume as a function of mass together with velocity curves. This model is to be used in the design of space vehicles which will travel in interplanetary space or will orbit planets. Also given is a simplified model and sample applications of both models to a space vehicle mission (appendix A). A glossary is presented in appendix B.

The meteoroid environment for use in the design of space vehicles operating from near Earth to the lunar surface is given by another design criteria monograph in this series (ref. 1).

Monographs on Jupiter and Saturn are in preparation which will include meteoroid conditions peculiar to those planets.

2. STATE OF THE ART

Much of the state of the art concerning meteoroids from near Earth to the lunar surface is covered in reference 1. For convenience, appropriate sections of that monograph are reproduced herein together with additional analyses that are applicable to interplanetary space.

Present knowledge of both the occurrence and physical properties of meteoroids is based primarily on Earth based observations of meteors, comets, asteroids, zodiacal light, as well

as on direct measurements of the meteoroid flux (number of particles per unit area per unit time) by instrumented sounding rockets and spacecraft. None of these methods of observation measure the meteoroid flux as a function of mass directly. In each case, the measured parameter (e.g., light intensity) must be interpreted through assumptions, other data, and characteristics of the observing instrument to determine meteoroid mass and velocity distributions. References 2 through 10 contain a review of these observations.

2.1 Observations and Measurements

2.1.1 Photographic Observations

Photographic observations have furnished the best information on meteors to date. The meteoroid population is inferred from analysis of photographic meteor observations. As a meteoroid enters the Earth's atmosphere, a certain fraction (the luminosity coefficient) of its kinetic energy is converted to light. If the angular velocity and altitude of the meteor is known, a single photograph will determine the amount of light emitted by the meteor; hence, if the luminosity coefficient is known, the meteoroid's original kinetic energy can be determined. In addition, the meteor velocity and deceleration can be determined by triangulation with two cameras. References 11 through 14 contain the data generally conceded to be the best estimates of the flux of meteors as a function of particle luminosity. The meteoroid population inferred from these observations, however, is subject to error because of several limitations in the data such as the following: only Earth-crossing meteoroids are observed; a restricted range of masses is covered; the conversion of luminosity measurements to mass is uncertain; and meteoroid composition and structure are not well defined.

The estimated mass range of photographic meteors is about 10^{-3} gram and larger.

2.1.2 Radar Observations

Radar observations of meteors have been obtained from the reflection of a radar beam by the ionized meteor trails. Analysis of the reflected radar beam gives the ionization and velocity of the meteor. This information is used in conjunction with meteor theory to show a relationship between meteor ionization and meteoroid mass. References 15, 16, and 17 contain some recent reviews of meteor influx rates based on radar observations.

Since clouds and daylight do not limit sampling periods for these observations as is the case for photography, the radar data should have more statistical significance. However, this technique has limitations similar to the photographic as well as others. These other drawbacks include an additional selection bias against very low and very high velocity meteors and against the disturbing effect of wind shear on the ionized trails of the fainter objects. Principally because of the more severe selection effects, the radar technique is considered less reliable than the photographic meteor measurements. The estimated mass range for radar meteors is from about 10^{-6} to 10^{-2} gram.

2.1.3 Direct Measurements

Meteoroid detectors mounted on spacecraft and rockets have furnished information on the meteoroid flux by measuring the momentum or penetration energy of meteoroids (refs. 5 and 7 through 10). Fluxes in the estimated mass range of 10^{-13} to 10^{-7} gram have been detected by acoustic impact (microphone) sensors, and fluxes in the mass range of 10^{-9} to 10^{-6} gram have been detected by complete penetrations (perforations) of thin metallic sheet sensors.

Measurements by acoustic impact sensors (refs. 5, 7, and 9) indicate a higher cumulative flux in the mass range of 10^{-7} gram and less than do the penetration sensors (refs. 7, 8, and 10). Although neither the acoustic nor penetration sensors directly measure meteoroid mass or velocity, the penetration sensors probably give a more accurate description of the meteoroid flux than either the photographic or radar data. Interpretation of the physical damage to penetration sensors is subject to errors in conversion from sensor thickness to meteoroid mass, but the penetration theory is probably better understood than meteor theory. Currently, there are still some unresolved questions concerning the interpretation of acoustic impacts.

2.1.4 Zodiacal Light

The surface brightness of the zodiacal light has been measured as a function of angle from the Sun and in several wavelength intervals. Polarization measurements have also been made. However, the measurements have proven insufficient to determine a unique meteoroid size distribution or how this distribution varies with distance from the Sun. References 18 through 23 are only a small sample of the many papers concerned with the zodiacal light. The size distributions found from these analyses are usually in vast disagreement because of differences in assumptions that are made. Nevertheless, the size distribution found from recent meteoroid measurements by the penetration satellites (ref. 24) is consistent with the intensities of zodiacal light (ref. 25).

2.1.5 Asteroids

Asteroids are observed by telescopes since the brightest one is just at the limit of visual sensitivity. Only the diameters of the four largest asteroids are measurable—the diameters of the remainder must be inferred from their brightness. For this reason, the brightness is usually reported in units of "absolute magnitude," which is the magnitude of the asteroid if it were placed 1 AU from the Sun and observed from the Sun. Studies of the intensity of asteroid brightness with time indicate that many asteroids are rotating and have irregular shapes. The orbits, positions, and absolute magnitudes of 1684 asteroids are given in reference 26. This reference represents the results of about 150 years of casual observations. A systematic survey of the asteroids was conducted by Kuiper, et al., (ref. 27) to determine the "completeness" of the cataloged asteroids. Reference 26 is probably complete to a mean

photographic opposition magnitude of 14. This corresponds to an asteroid 50 km in diameter at 2.8 AU with an assumed geometric albedo of 0.1.

2.1.6 Meteorites

Meteorites range in size from a few kilograms to about 10^6 kilograms and are believed to be of asteroidal origin. Efforts to determine the meteoroid flux from meteorites are complicated by the probability of seeing one fall and relating the mass of the meteorite found to its original mass. Estimates of the meteorite flux on Earth are given in references 28 and 29. Recently, two networks have been established to photograph large meteors (fireballs): one in the United States (Prairie Network, ref. 30), and one in Czechoslovakia (ref. 14). Their purpose is to determine the orbits of meteoroids and recover surviving meteorites. Recovery has been successful twice (refs. 31 and 32). On the basis of structure and composition, meteorites are classified as irons and stones (ref. 4). There is some evidence that stony meteorites may be of cometary origin (ref. 33).

2.2 Asteroid Mass Distribution

The largest uncertainty in the meteoroid environment between the orbits of Mars and Jupiter is the asteroid mass distribution. Asteroids are inferred to have diameters from a few kilometers to a few hundred kilometers. The presence of these larger bodies suggests the presence of smaller, unobservable bodies. When asteroids collide, fragments are produced which eventually collide again with other fragments. Because of this continuous collision process, much smaller asteroids most likely exist. Such asteroids could pose considerable danger to spacecraft if present in sufficient number.

Various methods have been used to predict the number of smaller bodies in the asteroid belt. These methods include estimates of the mass distribution that follow from lunar and Martian crater distributions (refs. 34 to 38), meteorite finds (refs. 28 and 29), and theoretical and experimental studies of rock crushing laws (refs. 39 to 41). The number of smaller asteroids can also be estimated by the trend set by the larger ones. Most analyses indicated that the number of asteroids of mass m and larger (the cumulative mass distribution) varies as $m^{-\alpha}$ where α is a constant. In extrapolating from the larger asteroids, a greater value for α indicates a larger number of smaller asteroids.

Several difficulties arise in interpreting lunar and Martian crater counts into asteroidal influx rates: (1) The age of the impacted surface is unknown. (2) It is not known whether the craters were formed by asteroids, comet nuclei, secondary ejecta, or volcanism. (3) The surface features of craters are eroded (by smaller meteoroids on the Moon or by wind on Mars), causing the smaller craters to disappear more rapidly than larger craters. (4) A surface can become saturated so that larger craters will obliterate a significant number of smaller craters. When this occurs, the number of impacting particles cannot be determined, and the original distribution is difficult to determine. Saturation appears to have taken place on the surfaces of Mars and the lunar highlands (refs. 37 and 38).

If meteorites are assumed to be of asteroidal origin, there are still problems of relating a meteorite mass to its original mass because of ablation and fragmentation. Hawkins (ref. 28) deduced the mass distribution of stony and iron meteorites and predicted their cumulative mass distribution "in space" to vary as m^{-1} and $m^{-0.7}$, respectively. Brown (ref. 29), on the other hand, found both stones and irons to vary as $m^{-0.77}$.

Several authors have attempted to predict the number of smaller asteroids by theoretical and experimental studies of the effects of collisions between rocks. Piotrowski (ref. 39) found that under certain restrictive conditions, erosion and breakup of asteroids would lead to a cumulative mass distribution varying as $m^{-2/3}$. Hawkins (ref. 40), however, pointed out that as terrestrial rocks are crushed, the value of a increases and approaches -1. Dohnanyi (ref. 41) used experimental results of hypervelocity impacts to determine a rock crushing law for the asteroids and their debris. He found that a steady-state solution exists when the cumulative mass distribution varies as $m^{-0.84}$. Dohnanyi also points out that his results are consistent with the observed asteroids in reference 27.

Since any asteroidal component in the zodiacal light (or any other observed phenomenon) cannot be greater than the total observed brightness, upper limits of the number of smaller asteroids can be set by use of certain assumptions. In reference 42, Kessler uses the dim light of the gegenschein to estimate an upper limit.

2.3 Meteoroid Velocity

Relative meteoroid velocities are a function of the spacecraft velocity and position as well as the orbits of the meteoroids. Cometary meteoroid orbits are found in reference 43, and asteroid orbits are found in reference 26. However, both these data contain selection effects.

Most meteoroid velocity studies treat mainly the velocity distribution relative to the Earth. (These velocities range from 11 to 72 km/sec.) The major problem occurs in correcting the data for selection effects. Typical distributions of meteor velocities relative to the Earth from photographic measurements (refs. 3, 43, and 44) show two peaks. The second peak in the distribution is attributed to meteoroids in retrograde orbits. However, their higher entry velocities are more easily detected than those of the slower direct orbit meteors. This selection effect distorts the relative number of meteors in direct and retrograde orbits. A velocity distribution corrected to a constant mass is obtained in references 45 and 46 by compensating for the velocity bias inherent in the photographic technique. Average velocity values, determined from photographic measurements are 20 km/sec by Dohnanyi (ref. 45); 17 and 15 km/sec by Kessler (ref. 46) for a gravitating and nongravitating Earth, respectively; 19 km/sec by Dalton (ref. 47); 22 km/sec by Whipple (ref. 48); and 30 km/sec by Burbank et al. (ref 49).

The velocity distributions of the measured radar meteors do not, to the same extent, exhibit the bi-modal shape characteristics of the photographic meteors. The high velocity peak is not attained because the more numerous smaller meteors leave a diffused ionized wake. Recent unpublished distributions, obtained by the Harvard College Observatory and

Smithsonian Astrophysical Observatory with the radar technique, indicate a higher average velocity for meteoroids smaller than those detectable by the photographic technique. When an attempt is made to remove the selection effects (as was done for the photographic data), the average velocity derived from the radar distributions decreases to a value nearer that obtained from the photographic measurements.

The Earth's gravity causes another selection effect on both the photographic and radar meteors. Meteoroids are "pulled in" and accelerated by the Earth; slower meteoroids are affected more than faster ones. Kessler (ref. 46) removes these effects to determine the average velocity in interplanetary space.

The selection effects involved in the observed asteroids (ref. 26) are less important in determining average asteroid velocities. Asteroids near the Earth are more likely to be discovered than those at greater distances. Kuiper (ref. 27) found that this selection effect was essentially a function of the asteroid's orbital semi-major axis. However, before relative velocities can be computed, each asteroid orbit must be weighted by the probability of collision with a spacecraft (ref. 50).

2.4 Meteoroid Density

The mass density of cometary meteoroids is highly uncertain. This parameter (as in the case of meteoroid mass) is not a measured quantity; it is derived from theory and assumptions. The cometary meteoroid has been described by Whipple in reference 51 as a conglomerate of dust particles bound together by frozen gases or "ices," whereas Öpik (quoted in reference 51) has postulated a dust-ball. Each author assumed a mass density less than 1 g/cm^3 in developing a flux-mass relationship. Values of average density calculated from photographic and radar observations (refs. 48, 52, 53, and 54) have ranged from 0.16 to 4 g/cm^3. In assessing the available density data, related assumptions, and calculation procedures, it was taken into consideration (in accordance with Whipple) that the lower densities obtained from radar observed meteor data were not reliable and the higher densities were not typical of cometary debris. From the assessment, 0.5 g/cm^3 was chosen as the value for the mass density of meteoroids of cometary origin even though this value may be somewhat low or nonconservative.

Meteorites are generally considered to have been meteoroids of asteroidal origin. Mass densities for meteorites range from about 3 or 4 g/cm^3 for most stones to 7.8 g/cm^3 for irons (ref. 6). At smaller mass sizes (a few kilograms), stony meteorite finds are much more abundant than iron meteorites (ref. 28). The low crushing strength of some of these stones has led to speculation that the influx of these meteoroids is even much higher than indicated by stone finds. In view of these considerations, an average mass density of 3.5 g/cm^3 for meteoroids of asteroidal origin has been adopted.

2.5 Variations in Spatial Density

The spatial density (number per unit volume) of meteoroids varies throughout space as a function of distance from the Sun, distance from a planet, and ecliptic latitude and longitude. These variations can be as large as several orders of magnitude. Localized variations may exist in the form of meteoroid streams; however, there is insufficient data to construct a model describing their intensity and position in space.

2.5.1 Variation in Spatial Density with Distance from the Sun (Radial Distribution)

2.5.1.1 Cometary Meteoroids

The consenus of opinion is that photographic meteors, radar meteors, and the zodiacal light are phenomena caused by cometary meteoroids (refs. 55 and 56). Briggs (ref. 57) and Southworth (ref. 58) have studied orbit distribution of photographic and radar meteors. They conclude that the spatial density of cometary meteoroids varies as $R^{-1.0}$ to $R^{-1.5}$ where R is the distance from the Sun in AU. A similar conclusion is reached by analysis of the zodiacal light (refs. 18 and 22) where $R^{-1.5}$ is a favored result.

2.5.1.2 Asteroidal Meteoroids

For lack of data, the radial distribution of asteroidal meteoroids is assumed to be the same as that of the observed asteroids in reference 26. Narin (ref. 59) calculated the position of the observed asteroids on a series of particular days and hence determined their radial distribution. However, he did not correct for the observational selection effect mentioned in section 2.3. Kessler (ref. 60) computed the probability of finding an asteroid at given distances from the Sun and then produced a series of graphs to give the spatial density of asteroids as a function of asteroid size for various distances from the Sun. From these graphs, the radial distribution can be determined for a given mass range of asteroids.

2.5.2 Variation in the Meteoroid Flux Near a Planet

It is more convenient to speak of the changes in meteoroid flux (number of impacts per unit area per unit time) as a planet is approached than to speak of the changes in spatial density (number per unit volume). An increase in meteoroid flux is the result of a planet's gravitational attraction. A decrease in flux results from the shielding offered by the planet, and this can be expressed simply as the fraction of solid angle subtended by the planet (ref. 1).

By considering conservation of energy and angular momentum, Öpik (ref. 61) found the gravitational increase in flux near a planet to be a function of the meteoroid velocity. If the

velocity distribution is a function of direction relative to the planet, then the gravitational increase in flux will also be a function of direction (ref. 62). However, only the average flux increase over the planet's surface will be considered here. By using the velocity distribution from reference 43 (this velocity distribution has an average velocity of 30 km/sec and has not been corrected for observational selection effects), Dycus, Bradford, and Luebbe (ref. 62) found that the ratio of flux at earth to that outside Earth's sphere of influence is 1.28. Dohnanyi found a ratio of 1.81 in reference 45. Reference 1 shows the ratio to be 1.76.

2.5.3 Variation in Spatial Density with Heliocentric Latitude and Longitude

2.5.3.1 Cometary Meteoroids

If the spatial density of cometary meteoroids varied with heliocentric longitude, it would be observed as a seasonal variation in the influx of meteors on the Earth's surface and as a seasonal variation in the intensity of the zodiacal light. Such variations in meteor influx rates have been observed (ref. 15) but are usually small (less than a factor of 2) and sometimes contradictory. Seasonal variations in the intensity of the zodiacal light are difficult to measure and hence controversial (ref. 63). Thus, although a longitudinal variation in cometary particles possibly exists, it is probably small and will be ignored in this monograph.

The heliocentric latitude distribution of cometary meteoroids has been inferred from photographic meteors (ref. 57), radar meteors (ref. 58), and zodiacal light (ref. 18). The latitude distributions from these sources are not in large disagreement.

2.5.3.2 Asteroidal Meteoroids

It has long been observed that the longitudes of perihelion (fig. B.2, app. B) of the asteroids tend to line up with the longitude of perihelion of Jupiter (about 14°). Such an alinement causes the asteroid belt to be closer to the Sun for this heliocentric longitude. Kresak (ref. 64) computed the distribution of heliocentric distances at which individual asteroids cross the longitude of Jupiter's perihelion and aphelion. He estimated that the spatial density of asteroids between 1.5 and 1.7 AU from the Sun in the direction of Jupiter's perihelion is one order of magnitude higher than in the opposite direction. Kessler (ref. 60) presents spatial density of asteroids as a function of absolute magnitude for various distances from the Sun and heliocentric longitude intervals. From these graphs a longitudinal variation in spatial density can be found.

2.6 Development of a Cometary Meteoroid Model

The meteoroid model developed in "Meteoroid Environment Model-1969 (Near Earth to Lunar Surface)" (ref. 1) is adopted here as the cometary meteoroid environment for near

Earth. The presence of meteoroid streams in interplanetary space may produce a large increase in flux at some point along the spacecraft trajectory. However, the average flux along the entire trajectory is considered by using the total (streams plus sporadic) meteoroid model in Reference 1 Slight modifications are necessary before this model can be used to represent the meteoroid environment in interplanetary space.

2.6.1 Mass Distribution

Reference 1 uses the data from the photographic meteors and penetration sensor satellites to obtain the total cometary meteoroid flux at Earth as

$$\left.\begin{aligned} \log_{10} F_c &= -14.37 - 1.213 \log_{10} m \\ &\text{for} \quad 10^{-6} \leq m \leq 10^{0} \\ \log_{10} F_c &= -14.339 - 1.584 \log_{10} m - 0.063 (\log_{10} m)^2 \\ &\text{for} \quad 10^{-12} \leq m \leq 10^{-6} \end{aligned}\right\} \qquad (1)$$

where F_c is the number of cometary meteoroid impacts of mass m grams and larger per square meter per second. These fluxes must be multiplied by 0.565 (ref. 1) to obtain the flux at 1 AU without the effect of Earth's gravity.

The meteoroid flux is proportional to the spatial density (number of meteoroids per unit volume) and the relative velocity between the spacecraft and meteoroid. This relative velocity is a function of the heliocentric spacecraft velocity vector and the meteoroid velocity vector. Since this model applies to all spacecraft velocity vectors, equations (1) must be expressed as spatial density. In section 2.6.2 the relative velocity variation with spacecraft velocity vector is determined. Spatial density is related to flux on a randomly oriented flat surface as

$$S = 4F \int_V \frac{n(V)\, dV}{V} = 4F \overline{V^{-1}} \qquad (2)$$

where V is the relative velocity in meters/sec between the spacecraft and the meteoroid and n(V) is the fraction of meteoroids impacting with velocity V. The factor of 4 is a result of random orientation.

Thus, the spatial density at 1 AU is found by letting F and n(V) in equation (2) be the flux and velocity distribution, respectively, relative to a zero-gravity Earth. Velocity distributions relative to zero-gravity objects in orbit around the Sun are derived in section 2.6.2. The value of $\overline{V^{-1}}$ for a zero-gravity Earth is found from this section by allowing R = 1.0 AU, θ = 0, σ = 1.0, and n = −1.0; the value is then $1/(14.3 \times 10^3$ m/sec).

Thus, multiplying equations (1) by 0.565 and changing to spatial density by using equation (2) with $\overline{V^{-1}} = 1/(14.3 \times 10^3)$, the spatial density at 1 AU from the Sun, outside the Earth's sphere of influence, becomes

$$\left.\begin{aligned} \log_{10} S_c &= -18.173 - 1.213 \log_{10} m \\ &\text{for} \quad 10^{-6} \leq m \leq 10^{2} \\ \log_{10} S_c &= -18.142 - 1.584 \log_{10} m - 0.063 (\log_{10} m)^2 \\ &\text{for} \quad 10^{-12} \leq m \leq 10^{-6} \end{aligned}\right\} \qquad (3)$$

where S_c is the number of cometary meteoroids per cubic meter of mass, m, grams and larger. The mass range is extended to 10^2 grams. Equations (3) are shown in figure 1.

2.6.2 Relative Velocity

The meteoroid orbits given in reference 43 are used for determining the average cometary meteoroid velocity relative to a spacecraft as was done in reference 46. That is, the meteors in reference 43 are corrected to some limiting mass and weighted to remove the effects of the Earth's gravity. Encounter velocities are computed for various spacecraft heliocentric velocity vectors with a weighting factor to account for the probability of collision. The meteors in reference 43 are corrected to a limiting mass to give an average velocity of 20 km/sec at the Earth's surface.

Then (as in reference 46) consider a spacecraft at a distance from the Sun of R AU whose velocity vector is in the ecliptic plane. The speed of the spacecraft is σ (in units of the circular orbit speed around the Sun at R), and the velocity vector makes an angle, θ, with surface of an imaginary sphere of radius R. For cometary meteoroids, the arbitrary assumption is made that the distribution of eccentricities, inclinations, and the ratios of semi-major axes (fig. B.2, app. B) to distance from the Sun is independent of distance from the Sun. Each meteor in reference 43 is weighted to correct for a limiting mass size, for the Earth's gravity, and for the differences in probability of collision. Velocity distributions are then calculated as a function of σ and θ with R = 1.0, and the average velocity of each distribution, $\overline{U}_c$, is then found. Values for $\overline{U}_c$ are given in figure 2, or they can be

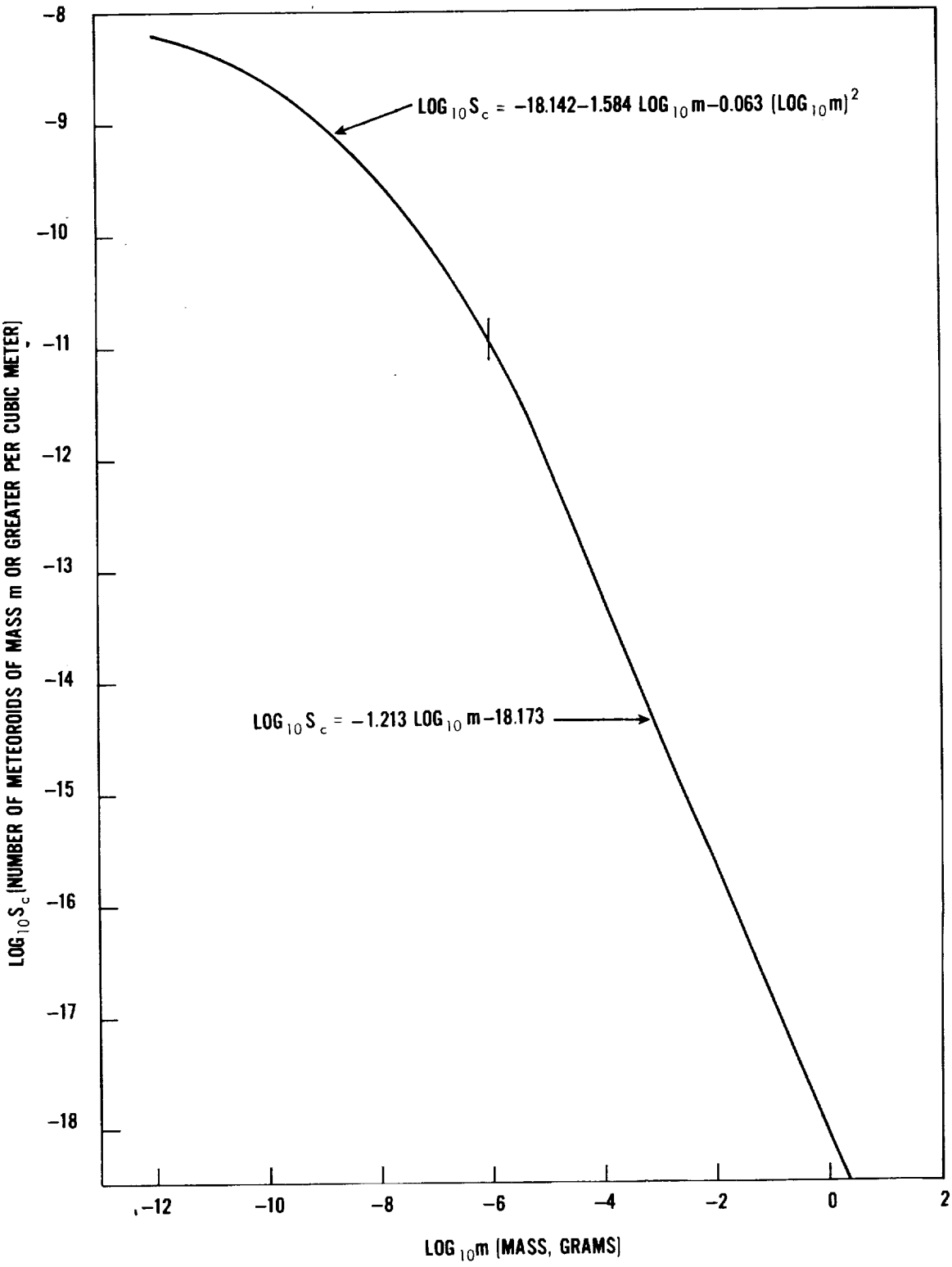

Figure 1. – Cometary meteoroid mass distribution at 1.0 AU.

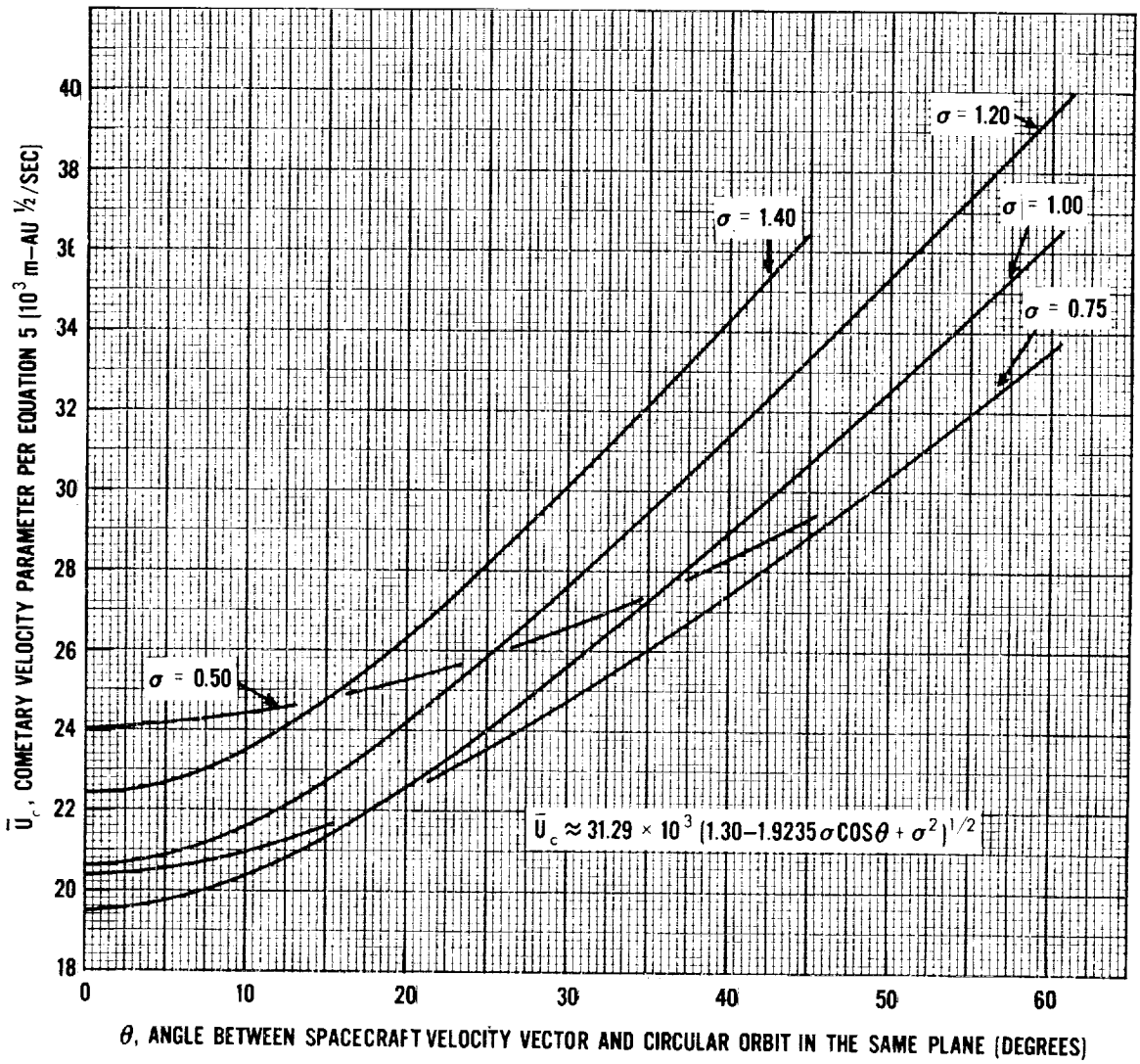

Figure 2. -- Average relative velocity of cometary particles where σ is the ratio of the heliocentric spacecraft speed to the speed of a circular orbit the same distance from the Sun.

approximated within a few percent (for $\overline{U}_c$ in m - $AU^{1/2}$/sec) by the expression

$$\overline{U}_c = 31.29 \times 10^3 (1.30 - 1.9235\, \sigma \cos\theta + \sigma^2)^{1/2} \quad (4)$$

The average cometary meteoroid velocity relative to the spacecraft, $\overline{V}_c$, as a function of R will then vary as

$$\overline{V}_c (\sigma, \theta, R) = R^{-1/2}\, \overline{U}_c (\sigma, \theta) \quad (5)$$

Most calculations require other weighted average velocities. The values of $\overline{V_c^{-1}}$, $\overline{V_c^2}$, and $\overline{V_c^3}$ were also calculated from each velocity distribution. These averages could each be presented in the same manner as $\overline{V}$ is presented. However, it was found that for each velocity distribution, these weighted average velocities could be approximated by the relationship

$$\left(\overline{V_c^n}\right)^{1/n} = \overline{V}_c\, \delta_c^{(n-1)/2} \quad (6)$$

where δ_c is only a function of the spacecraft velocity vector (i.e., θ and σ). Values for δ (θ, σ) are given in figure 3. Thus, from figure 3, the average velocity, $\overline{V}_c$, differs from the averages $\left(\overline{V_c^{-1}}\right)^{-1}$ and $\left(\overline{V_c^3}\right)^{1/3}$ by a maximum factor of about 1.4 for near circular spacecraft orbits. In general, the ratio approaches unity as the spacecraft orbit becomes more elliptical.

2.6.3 Radial and Latitudinal Distribution

In view of the observations of the photographic meteors, radar meteors, and zodiacal light (refs. 18 to 22, 57 and 58) a radial distribution varying with distance from the Sun by $R^{-1.5}$ has been adopted. The same data indicate that the variation in spatial density of cometary meteoroids with heliocentric latitude, β, can be approximated by the function, $e^{-2\,|\sin\beta|}$. With the assumption that these two distributions are independent of each other and the mass distribution, the terms, $-1.5 \log_{10} R - 0.869\, |\sin\beta|$, are added to equations (3) to obtain the spatial density of cometary meteoroids at distance R AU from the Sun and heliocentric latitude β.

2.7 Development of an Asteroidal Meteoroid Model

2.7.1 Mass Distribution

The uncertainty in the mass distribution of asteroidal meteoroids constitutes the largest uncertainty in the interplanetary meteoroid model between the orbits of Mars and Jupiter. This uncertainty is illustrated in figure 4 where the spatial density of the observed asteroids at R = 2.5 (ref. 60) is compared with various models that have been discussed. If particles

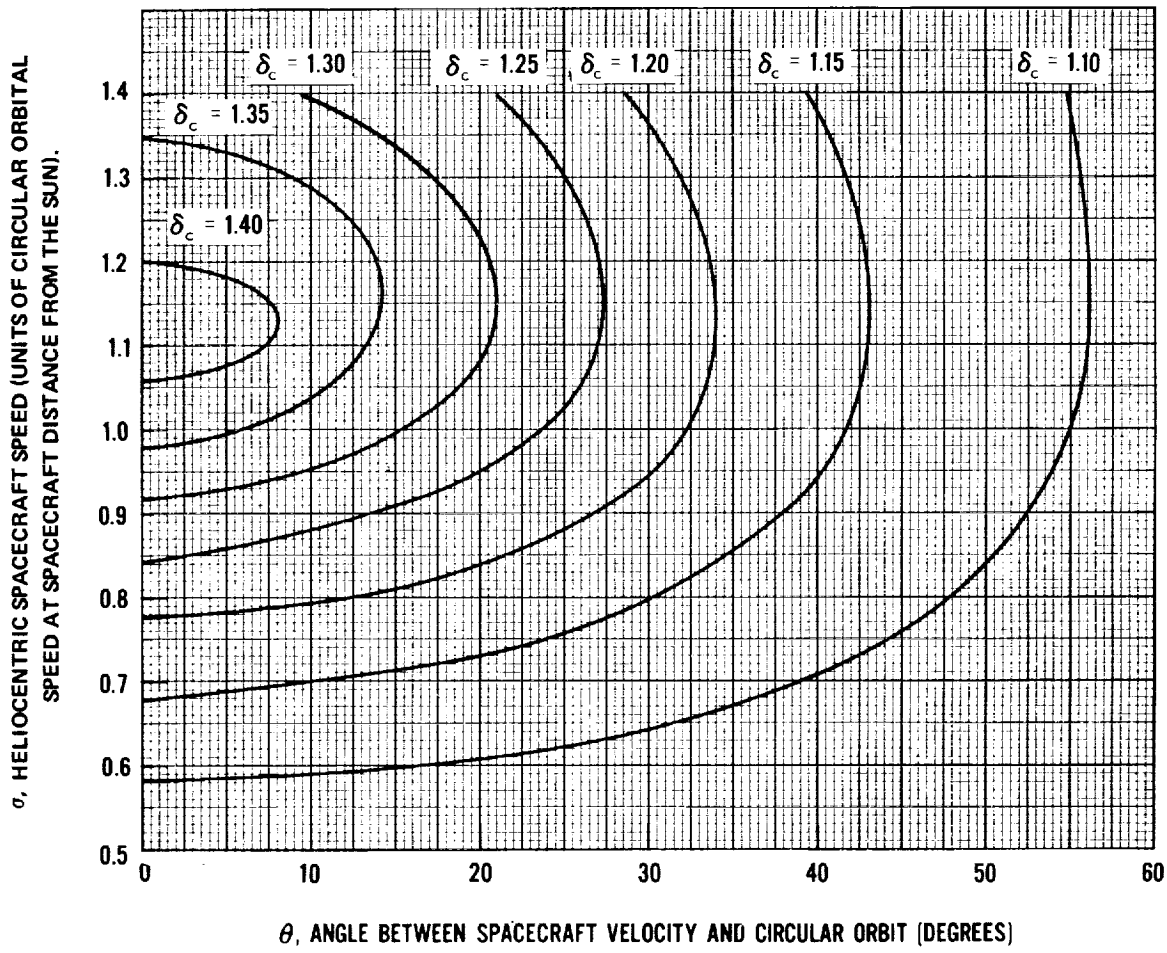

Figure 3. – Velocity parameter for weighted average velocities of cometary meteoroids where δ_c is the ratio of the average velocities $\left(\overline{V_c^n}\right)^{1/n}$ and $\left(\overline{V_c^{n-2}}\right)^{1/n-2}$, or, in general, $\left(\overline{V_c^n}\right)^{1/n} = \overline{V}_c\, \delta_c^{(n-1)/2}$

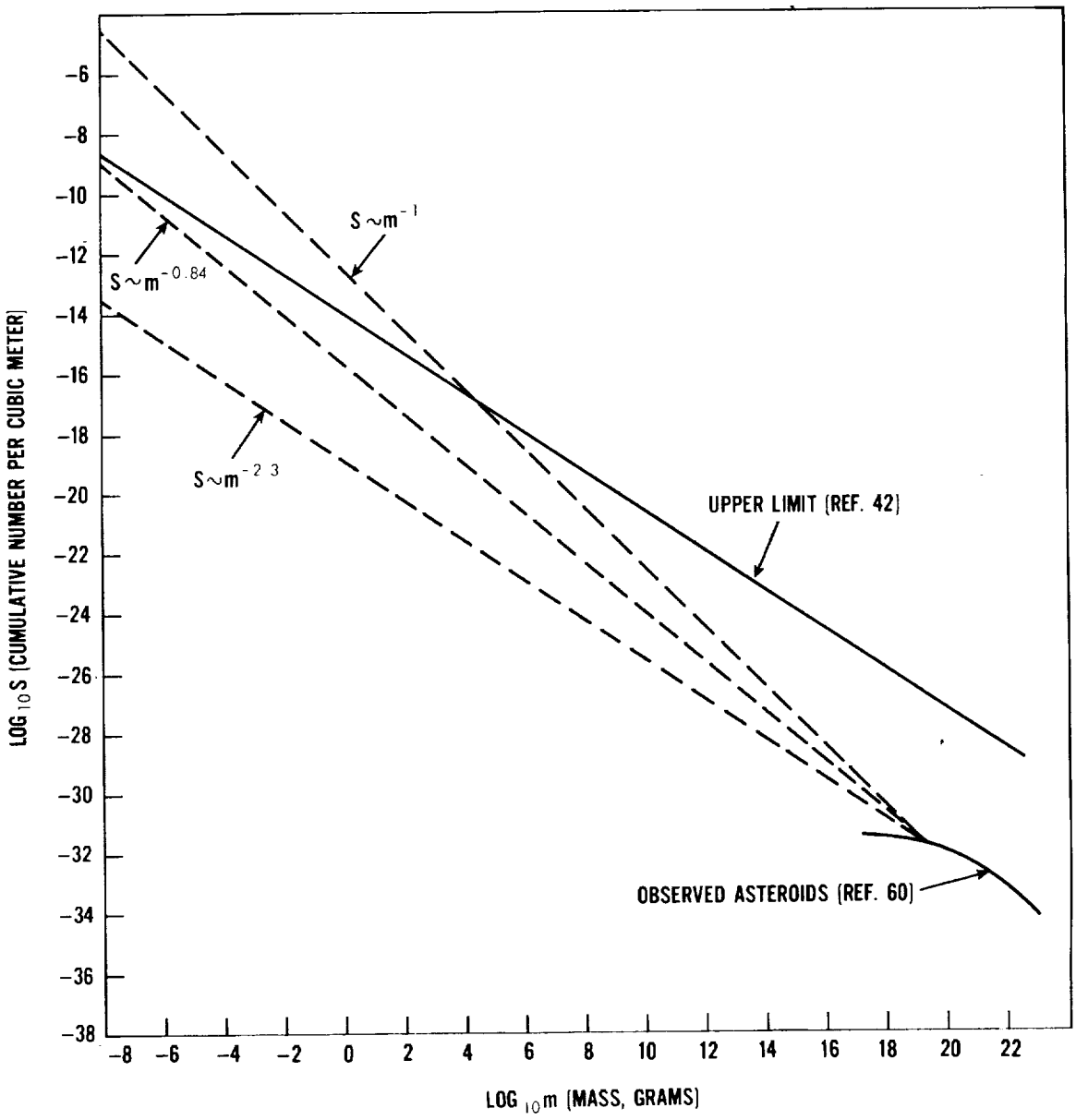

Figure 4. – Various asteroidal mass distribution models at 2.5 AU.

are spherical, asteroidal mass is related to its absolute magnitude in reference 65 by

$$\log_{10} m = 24.47 + \log_{10} \rho - 3/2 \log_{10} p - 0.6 M_0 \quad (7)$$

where ρ is the asteroid's mass density, p its geometric albedo, and M_0 its absolute magnitude. A mass density of 3.5 g/cm^3 has been assumed. The geometric albedo measured for five asteroids ranges from 0.1 to 0.4 (ref. 65); for Mars, Mercury, and the Moon, this albedo is about 0.1; and from zodiacal light studied, the albedo of dust particles is estimated to be less than 0.1 (refs. 19 and 66). Thus, a geometric albedo for asteroids of 0.1 was adopted which agrees with Kuiper, et al. (ref. 27) and Whipple (ref. 55).

For a spatial density greater than 10^{-15} or 10^{-16} particles per cubic meter, the probability of encounter must be considered for large spacecraft (i.e., a spacecraft with 500 m^2 of surface area exposed to the environment for 1 year). Therefore, if the spatial density of asteroids varies as m^{-1} (as suggested in reference 40 and shown in figure 4), such a spacecraft would require protection against impacts of masses as large as 10^3 grams. However, this mass distribution exceeds the upper limit set in reference 42 for masses less than 10^4 grams. If the mass distribution varies as $m^{-2/3}$ (ref. 39), the spacecraft would only have to be protected against asteroidal meteoroids of 10^{-5} gram (compared with cometary meteoroids of 10^{-3} or 10^{-2} gram).

The mass distribution suggested by Dohnanyi ($S \sim m^{-0.84}$) in reference 41 gives an intermediate result that is consistent with the upper limit for masses larger than 10^{-9}. When Dohnanyi's mass distribution is extrapolated from the larger asteroids in reference 60 at R = 1.0, the resulting flux comes within a few percent of the flux found by Whipple (ref. 55) from the Apollo asteroids, and the flux of meteoroids estimated from meteorite finds by Hawkins (ref. 28) and Brown (ref. 29). Such a mass law also gives consistent results with Öpik's prediction (also in ref. 55) that the ratio of the number of Mars to Earth crossing asteroids (of the same size) would be 300. This same mass distribution is found from the graphs given in reference 40 for masses larger than 10^{21} grams and smaller than 10^{19} grams. However, at approximately 10^{20} grams, the distribution curves flatten as shown in figure 5. This flattening appears to be real and has been considered in developing a model.

Thus, in this monograph it is assumed that the spatial density varies as $m^{-0.84}$ for masses between 10^{-9} and 10^{19} grams, the average geometric albedo of asteroids is 0.1, and the average mass density is 3.5 g/cm^3. The average effect of flattening around 10^{20} grams (absolute magnitude 11) is shown in figure 5* (from ref. 60), which is a reproduction of the average spatial density at 2.0 AU. The figure is slightly modified to be more representative of other distances (R = 1.9 to 2.4) where the flattening is also clearly demonstrated.

*Private communications with Drs. Kuiper and Gehrels at the University of Arizona indicate that the flattening or knee may not be as pronounced as shown in figure 5.

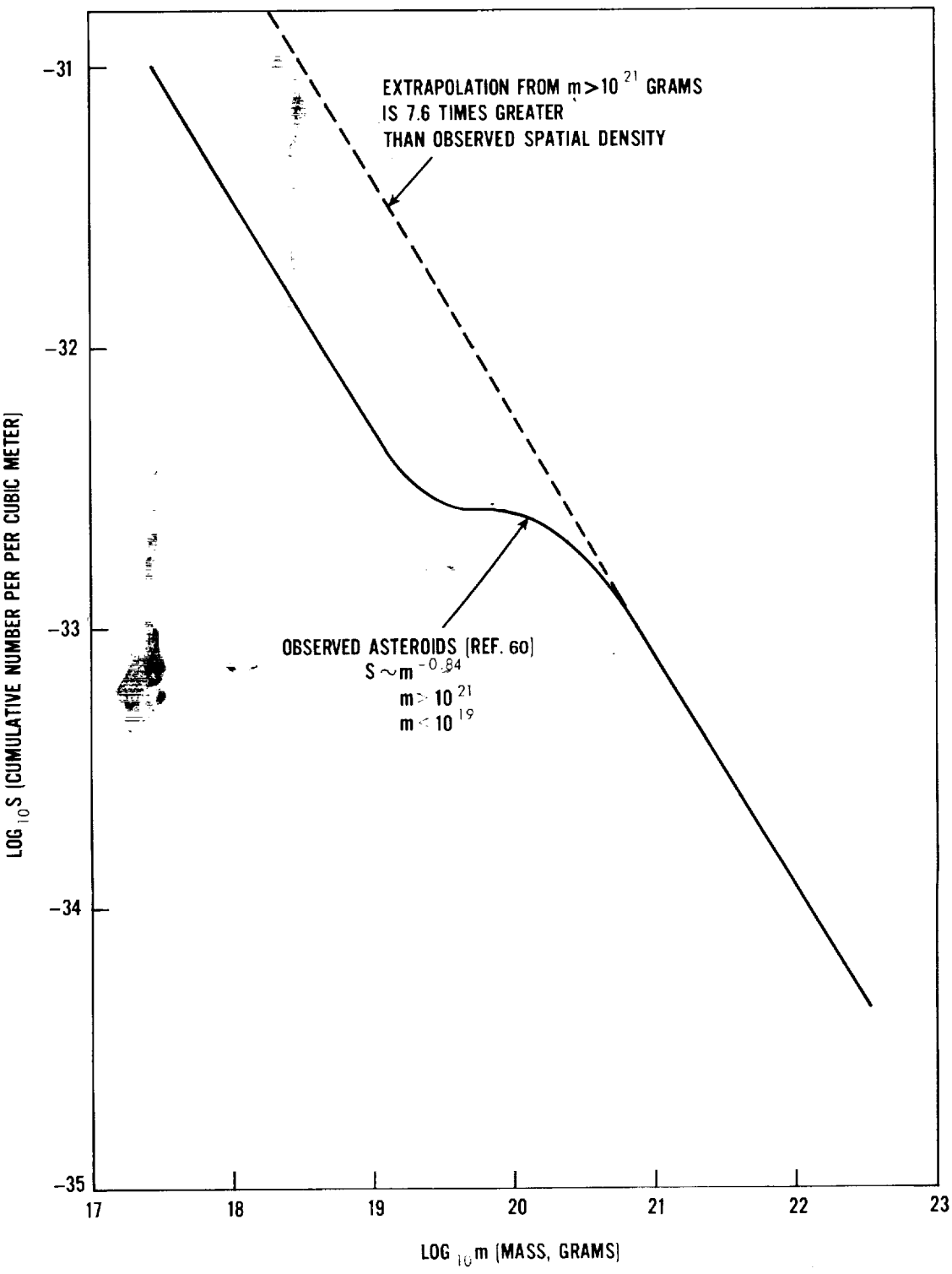

Figure 5. – Mass distribution of observed asteroids at 2.0 AU.

Thus, from reference 60, the spatial density at R = 2.5 for absolute magnitudes (M_0) less than 10, the spatial density in number per cubic meter is

$$\log S_a = 0.504\, M_0 - 37.18 \qquad M_0 < 10 \tag{8}$$

From figure 5, the spatial density of the smaller asteroids is 7.6 times less than equation 8, or

$$\log S_a = 0.504\, M_0 - 38.06 \qquad M_0 > 12 \tag{9}$$

By combining equations (7) and (9) with the adopted values of $\rho = 3.5$ and $p = 0.1$, the asteroidal spatial density at 2.5 AU becomes

$$\log S_a = -0.84 \log m - 15.79 \qquad 10^{-9} \leq m \leq 10^{19} \tag{10}$$

Equation (10) is shown in figure 6 for the masses in the range of interest to spacecraft designers. The equation is limited to masses larger than 10^{-9} gram for two reasons: (1) If this mass distribution is extrapolated to masses smaller than 10^{-9}, the upper limit in reference 41 would be exceeded. (2) Solar radiation pressure and the Poynting-Robertson effect would probably cause the mass distribution between 10^{-12} and 10^{-6} gram to change in a manner similar to the cometary meteoroids in the same mass region. Such a change can be approximated by limiting the distribution to asteroids of 10^{-9} gram or larger. To use a curved function similar to the cometary meteoroids, would imply more knowledge of the asteroidal mass distribution than is available.

2.7.2 Variations in Spatial Density

2.7.2.1 Radial and Longitude Distributions

The radial (variation in spatial density with distance from the Sun) and longitudinal (variation in spatial density with heliocentric longitude) distributions are found from reference 60 by comparing the spatial density of equal-size asteroids at various distances from the Sun and heliocentric longitude intervals. As suggested in section 2.7.1, the mass

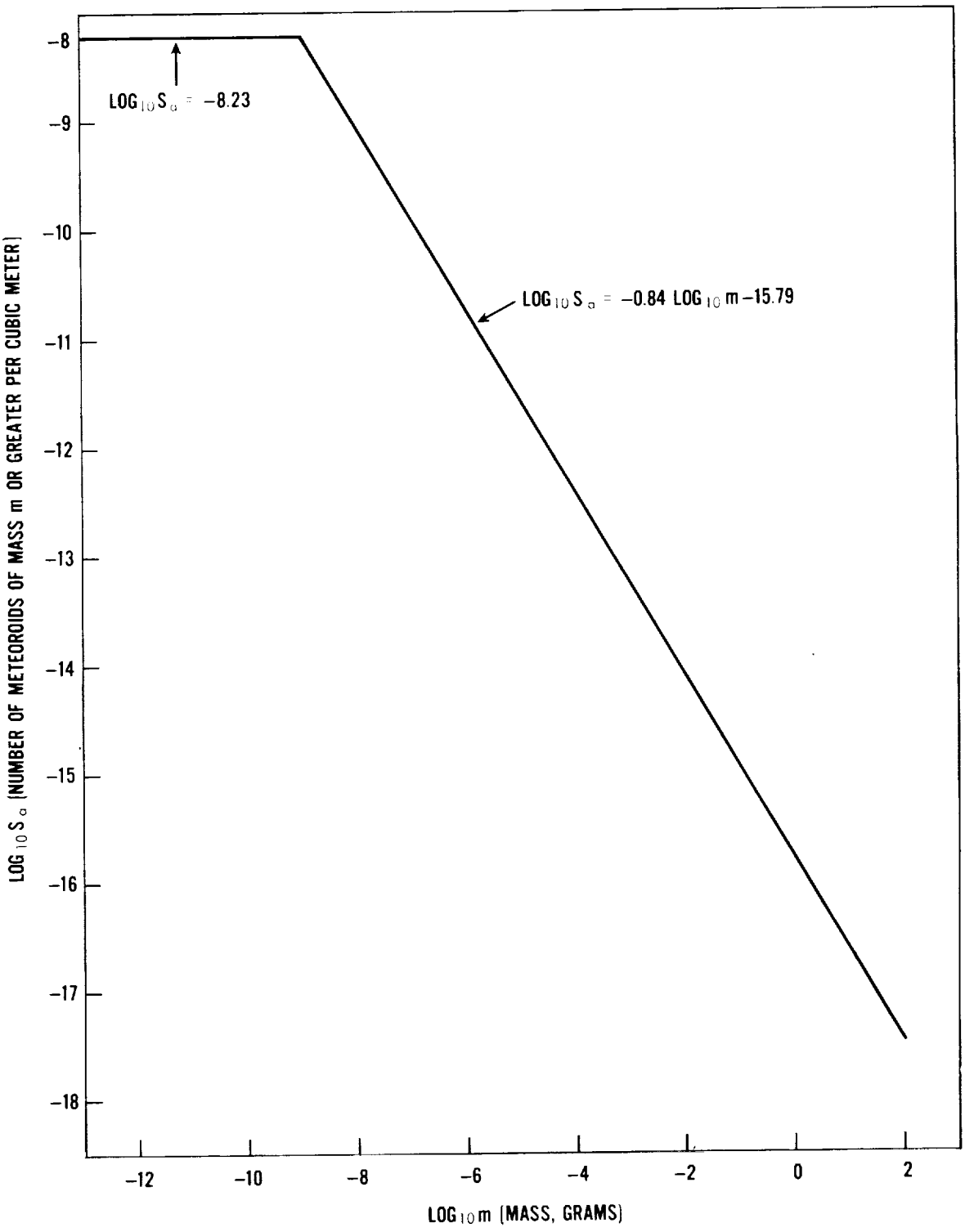

Figure 6. – Asteroidal meteoroid mass distribution at 2.5 AU.

distribution is assumed to be independent of distance from the Sun and heliocentric longitude. This leads to a spatial density expressed as

$$\log S_a (m, R, \lambda) = -0.84 \log m - 15.79 + f(R) + j(\lambda, R) \qquad (11)$$

where f(R) is the radial distribution, and j(λ, R) is longitudinal distribution. The spatial density as a function of heliocentric longitude, λ, may also be a function of R.

By using reference 60 to compare the spatial densities at various heliocentric longitudes and holding R and m constant, it is found that the log of the spatial density varies as g cos $(\lambda - \lambda_0)$ where g is a constant and λ_0 is the longitude of maximum spatial density. By repeating this for a series of R, it was found that g is a function of R as shown in figure 7. For distances from the Sun greater than 2.5 and less than 1.5 AU, g = 0. Thus

$$j(\lambda, R) = g(R) \cos (\lambda - \lambda_0) \qquad (12)$$

where g(R) is given in figure 7. The value of λ_0 is found from the above analysis to be very nearly 0°.

The value of f(R) is then found by comparing equal size asteroids in reference 60 at λ = 90° for various distances from the Sun. The results from this process are very nearly the same as presented for a spatial density averaged over all values of λ as a function of R. The value of f(R) is shown in figure 8.

Thus, the spatial density of asteroids can be expressed as

$$\log S_a = -0.84 \log m - 15.79 + f(R) + g(R) \cos \lambda \qquad (13)$$
$$\text{for} \quad 10^{-9} \leq m \leq 10^{19}$$

where values for g(R) and f(R) are given in figures 7 and 8, respectively.

2.7.2.2 Latitudinal Distribution

The spatial density of asteroids away from the ecliptic plane is discussed in reference 60 as a function of R and in reference 59 averaged over all values of R. It is concluded from reference 60 that the latitudinal distribution is nearly independent of R; consequently, the distribution given by Narin in reference 59 has been adopted.

The $\log_{10}$ of the ratio, h(β), of spatial density at heliocentric latitude, β, to the spatial density in the ecliptic plane is given in figure 9 as a function of β. Thus, from equation 13

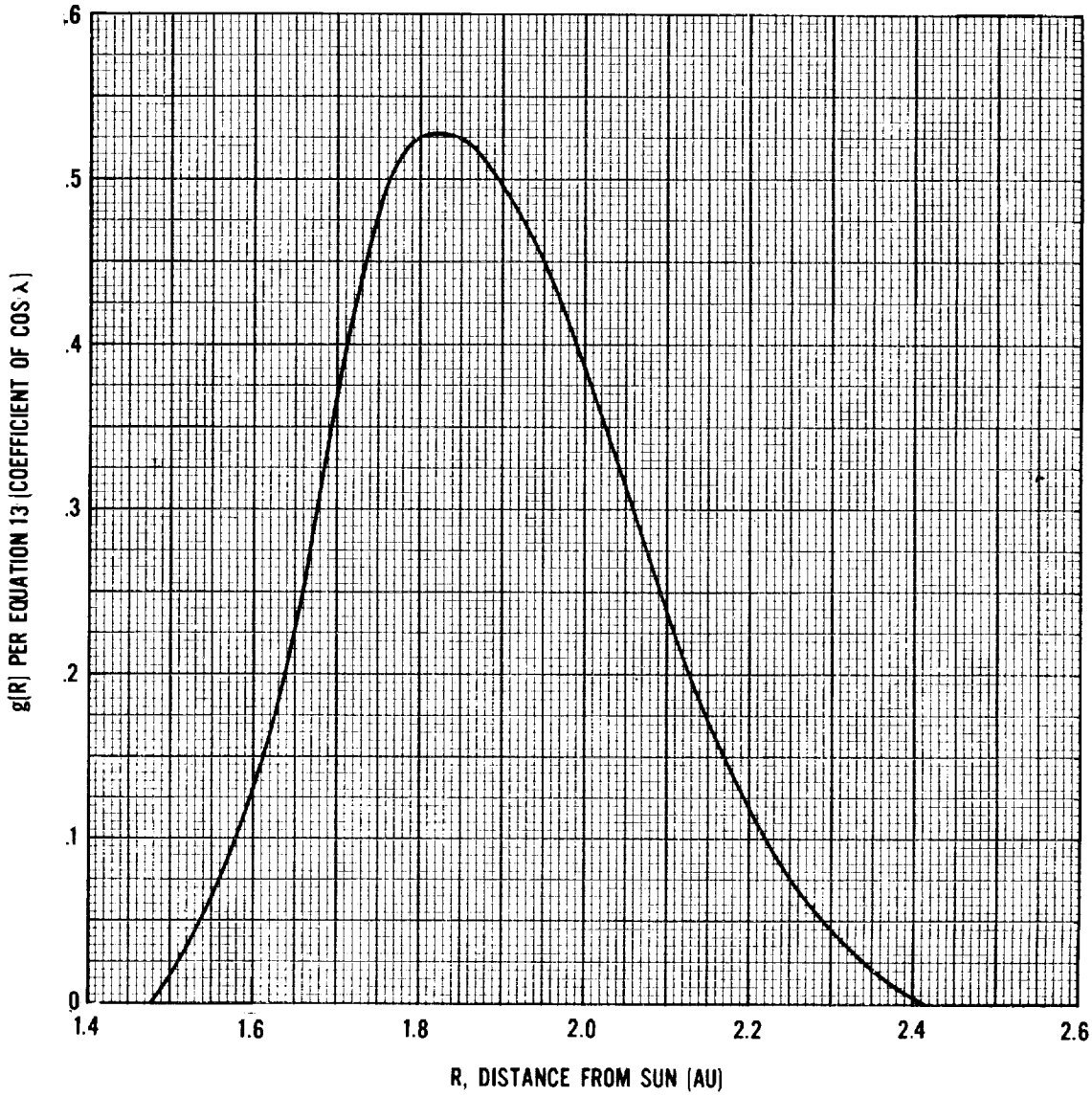

Figure 7. – Asymmetry of the asteroid belt with heliocentric longitude, λ (eq. 13).

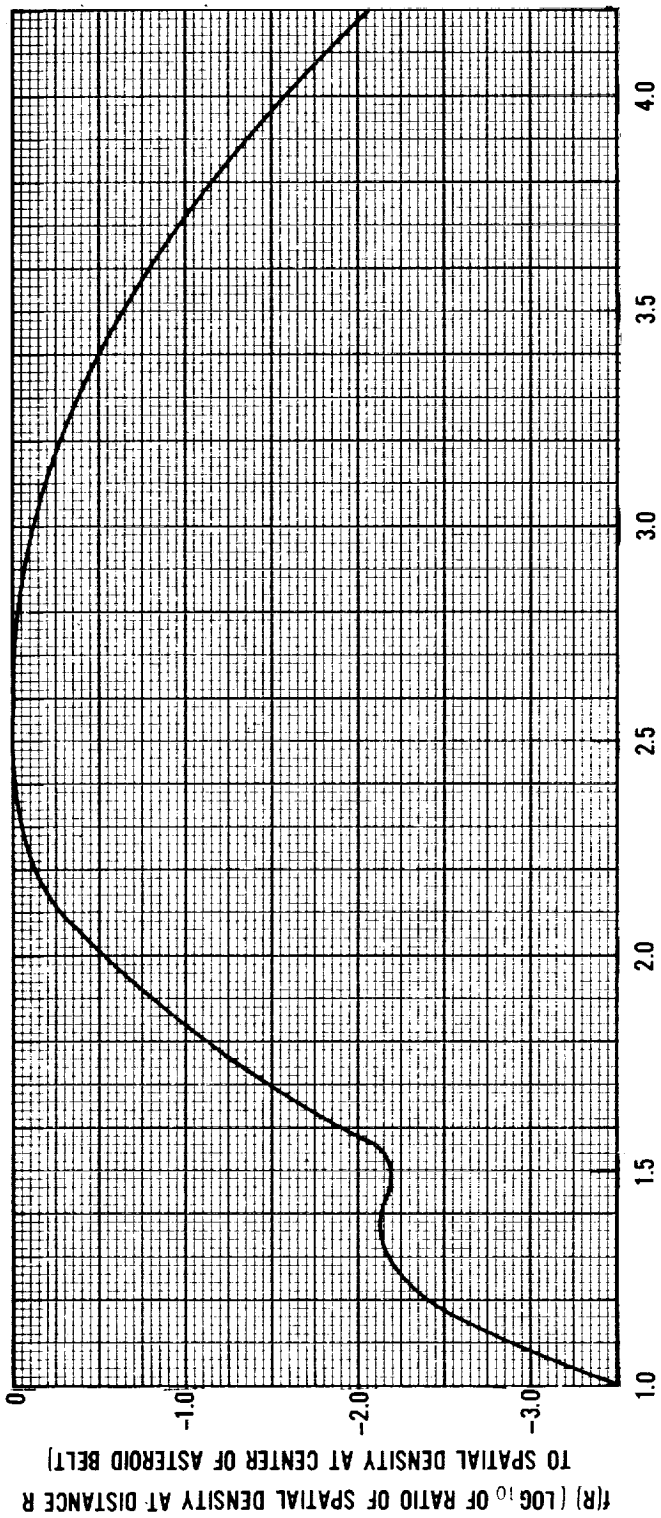

Figure 8. – Asteroid radial distribution (eq. 13).

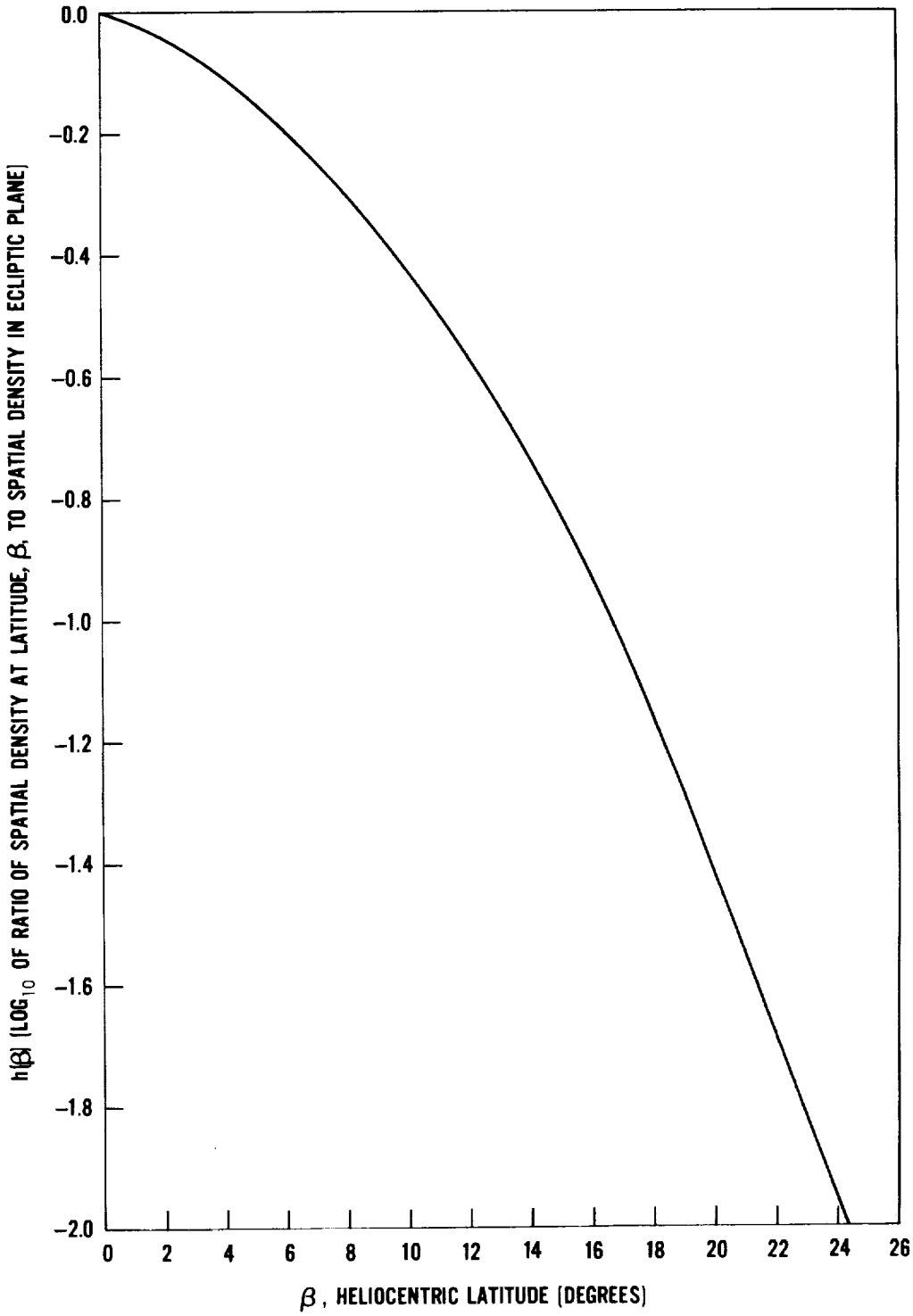

Figure 9. – Latitudinal distribution of asteroidal particles (eq. 13a).

the spatial density over all space is given by

$$\log_{10} S_a = -0.84 \log_{10} m - 15.79 + f(R) + g(R) \cos \lambda + h(\beta) \quad \text{for} \quad 10^{-9} \leq m \leq 10^{19} \tag{13a}$$

where $h(\beta)$ is given in figure 9.

2.7.3 Relative Velocity

The asteroids listed in reference 26 are used to determine the average impact velocity of asteroidal debris. The method is slightly different than that discussed in section 2.6.2 because of the differences between observational techniques for asteroids and meteors.

The asteroids must first be corrected to some limiting size. Kuiper (ref. 27) found that the probability of detecting an asteroid is primarily a function of its average apparent magnitude at opposition. This magnitude, in turn, is only a function of the asteroid's semi-major axis. Thus, the asteroids are corrected to some limiting size by a weighting factor that adjusts the relative number of asteroids with a given semi-major axis.

The probability of collision of each asteroid with the spacecraft is found by assuming that the distribution of argument of perihelion for asteroids is random. The probability of collision is then given by Wetherill in reference 50.

Thus, by using the asteroid orbits in reference 26, velocity distributions are obtained at distance R from the Sun for a spacecraft whose velocity vector makes an angle θ with the surface of an imaginary sphere of radius R. The speed of the spacecraft is σ, in units of the speed necessary to maintain a circular orbit of radius R around the Sun. The average asteroidal velocity, $\overline{V}_a$, is then found from each distribution. The velocity parameter

$$\overline{U}_a = \overline{V}_a R^{1/2} \tag{14}$$

is introduced and shown in figures 10, 11, and 12 for R = 1.7, 2.5, and 4.0 AU, respectively. These figures can be approximated by the following expressions where $\overline{U}_a$ is in m - $AU^{1/2}$/sec:

Figure 10, R = 1.7 AU

$$\overline{U}_a = 30.05 \times 10^3 (1.2292 - 2.1334 \sigma \cos \theta + \sigma^2)^{1/2} \tag{15}$$

Figure 11, R = 2.5 AU

$$\overline{U}_a = 29.84 \times 10^3 (1.0391 - 1.9887 \sigma \cos \theta + \sigma^2)^{1/2} \tag{16}$$

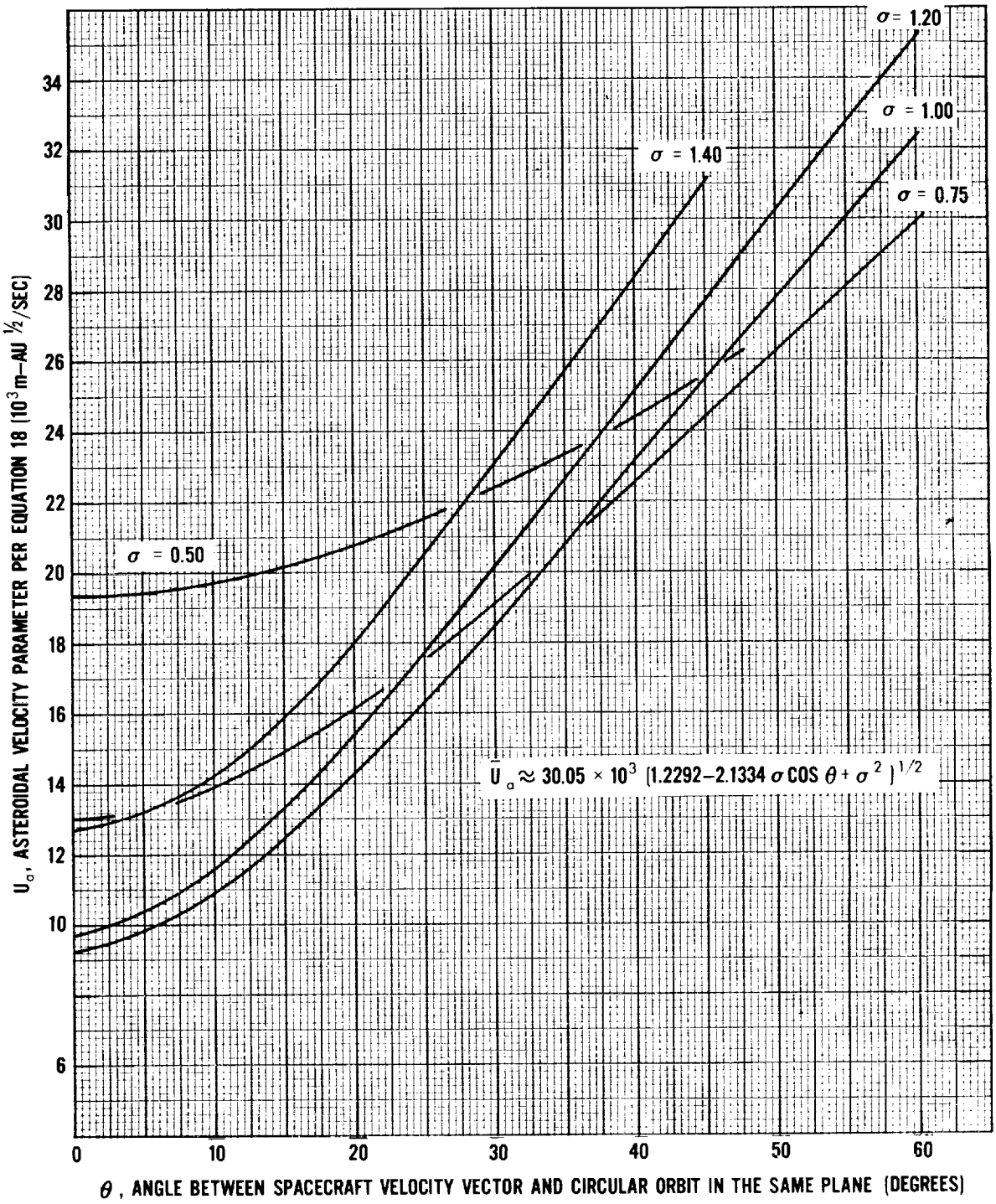

Figure 10. – Average relative velocity of asteroidal particles at R = 1.7 AU where σ is the ratio of the heliocentric spacecraft speed to the speed of a circular orbit the same distance from the Sun.

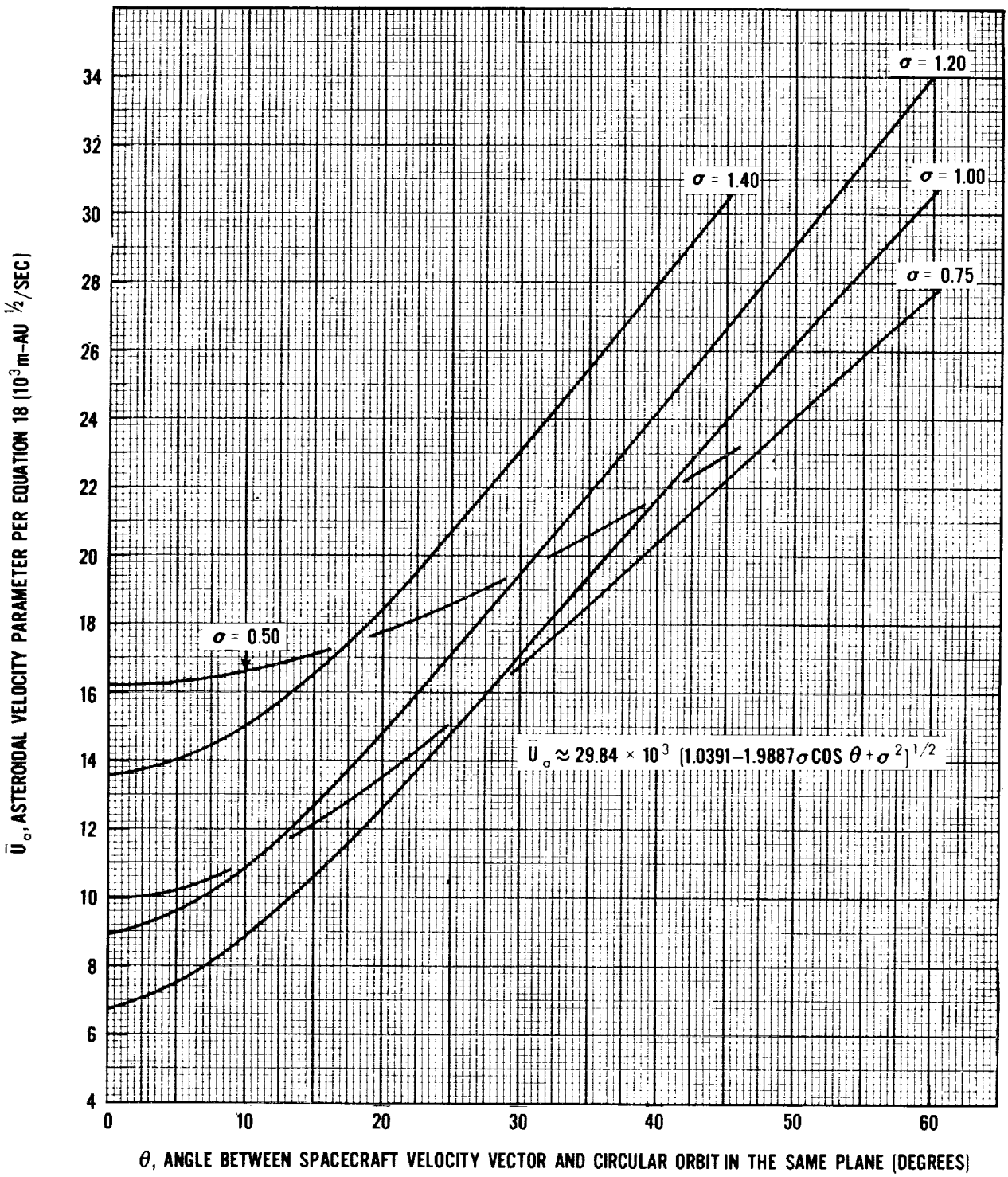

Figure 11. – Average relative velocity of asteroidal particles at R = 2.5 AU where σ is the ratio of the heliocentric spacecraft speed to the speed of a circular orbit the same distance from the Sun.

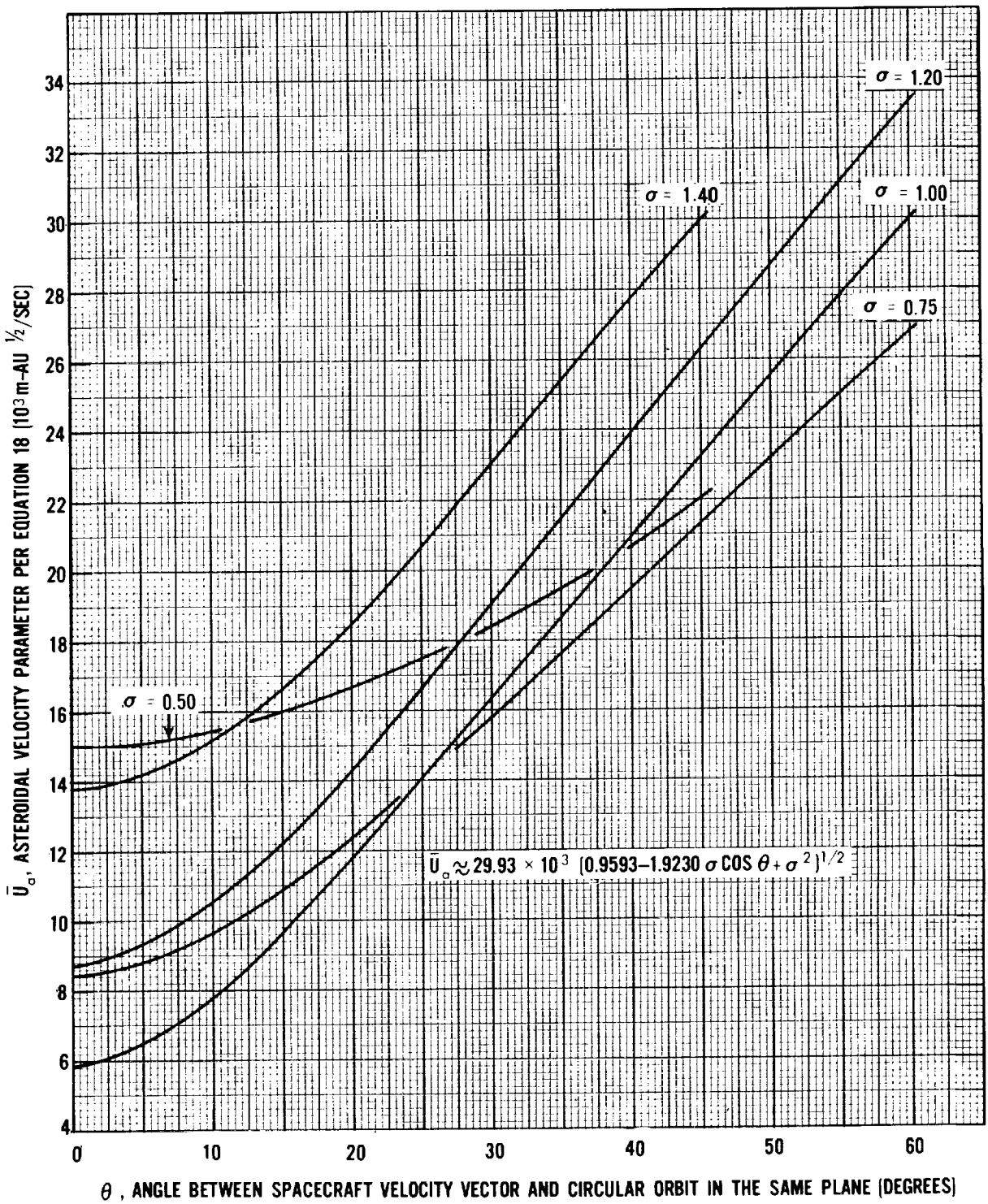

Figure 12. — Average relative velocity of asteroidal particles at R = 4.0 AU where σ is the ratio of the heliocentric spacecraft speed to the speed of a circular orbit the same distance from the Sun.

Figure 12, R = 4.0 AU

$$\overline{U}_a = 29.93 \times 10^3 (0.9593 - 1.9230\, \sigma \cos\theta + \sigma^2)^{1/2} \quad (17)$$

The velocity, $\overline{U}_a$, is introduced because it is not as sensitive a function of R as $\overline{V}_a$; thus, it is easier to interpolate between figures 10, 11, and 12.

The average asteroidal velocity is then

$$\overline{V}_a (R, \theta, \sigma) = R^{-1/2}\, \overline{U}_a (R, \theta, \sigma) \quad (18)$$

where $\overline{U}_a$ is shown in figures 10, 11, and 12.

As in the case of the cometary meteoroids (sec. 2.6.2), most calculations require weighted average velocities other than $\overline{V}_a$. These averages can be expressed as

$$\left(\overline{V_a^n}\right)^{1/n} = \overline{V}_a\, \delta_a^{(n-1)/2} \quad (19)$$

where δ_a is only a function of the spacecraft velocity vector, θ and σ. However, the asteroidal velocity distributions are so sharply peaked that almost all values of δ_a are very nearly equal to 1.0; this means that the weighted averages are equal to the average. The only exception occurs for spacecraft in very near circular orbits. For example, when R = 2.5 AU, σ = 1.0, and θ = 0, then δ_a = 1.2. However, by changing σ by only 0.2 or increasing θ by 15°, the value of δ_a drops to 1.1 and quickly approaches 1.0 for larger changes in σ and θ. Thus, use of the average asteroidal velocity alone will satisfy most calculation requirements.

2.8 Meteoroid Model Near a Planet

Other than shielding and gravity effects, it is assumed that the individual planets do not change the interplanetary meteoroid environment except as follows: (1) Meteoroids impacting the lunar surface induce "secondary" meteoroids which are described in reference 1. (2) The irregular satellites of the major planets, particularly Jupiter (reference 67), could produce "miniature asteroid belts" around such planets. Also, Saturn's rings pose a meteoroid hazard. Design criteria monographs concerning Jupiter and Saturn and their associated meteoroid environments are in preparation.

2.8.1 Shielding and Gravity Effects

For a spacecraft near a planet, the meteoroid flux is first calculated without the effects of the planet. Then the flux is multiplied by the factors developed below to account for planetary shielding and gravity enhancement.

2.8.1.1 Geometric Shielding

The flux encountered by a randomly oriented spacecraft is reduced by the fraction of solid angle subtended by a planet. This shielding factor was developed in reference 1 and here is expressed as

$$\eta = \frac{1}{2} + \frac{1}{2}(1 - r_p^2/r^2)^{1/2} \tag{20}$$

where r is the distance of the spacecraft from the center of the planet and r_p is the radius of the planet.

2.8.1.2 Gravitational Increase in Flux

Öpik (ref. 61) calculated that the ratio of meteoroid flux near a planet to the flux outside the sphere of influence of a planet is given by

$$G = 1 + V_p^2\, r_p/V^2\, r \tag{21}$$

where V_p is the escape velocity from the planet's surface and V is the unaccelerated velocity of the meteoroid relative to the planet. From the assumptions given in section 2.6.2 where R is the distance from the Sun in AU

$$V^2 = V_G^2/R \tag{22}$$

The unaccelerated velocity of the meteoroid relative to the Earth, V_G, is related to the accelerated velocity, V_∞, by

$$V_\infty^2 = V_G^2 + V_e^2 \tag{23}$$

where V_e is the escape velocity of the Earth.

Combining equations (22) and (23) with (21) and integrating this expression over the velocity distribution given in reference 1 yields

$$G = 1 + 0.76\, R\, V_p^2\, r_p/V_e^2\, r \tag{24}$$

where G is the ratio of the flux near a planet at distance R from the Sun to the flux at R if the planet were not present.

2.8.2 Meteoroid Velocity Near a Planet

Although a planet accelerates a meteoroid's velocity, it tends to pull in more of the slower moving meteoroids. The net effect for Earth, Mercury, Venus, and Mars is that the average velocity of captured meteoroids differs very little from average velocities in interplanetary space at the same distance from the Sun. For example, reference 1 gives the average velocity near the Earth's surface as 20 km/sec. Without the Earth's gravity, this average is only reduced to 19.4 km/sec (sec. 2.6.2). Similarly, the average velocities near Mercury, Venus, and Mars are within a few percent of the average found by neglecting the planets' gravity.

However, the large gravitational field near the larger planets (Jupiter, Saturn, Uranus, and Neptune) causes the average velocity relative to the planet to be essentially the same as the escape velocity of the planet.

The average velocity relative to the spacecraft can be approximated by the square root of the sum of the squares of the spacecraft and meteoroid velocity. Thus, for spacecraft near large planets, the average relative meteoroid velocity is given by

$$\overline{V} = \sqrt{\frac{r_p}{r} V_p^2 + V_s^2} \tag{25}$$

where r_p is the radius of the planet, r is the distance from the center of the planet, V_p the escape velocity from the planet's surface, and V_s the velocity of the spacecraft relative to the planet.

2.9 Meteoroid Directionality

Since the asteroids have nearly circular orbits, a spacecraft moving in a different orbit will encounter most of the asteroids coming from a single direction. A simple model can be set up to predict the direction by using the vector relationship between the spacecraft velocity and the circular asteroidal orbit in the ecliptic plane. Such a model has been tested against a more exact model employing all of the known asteroid orbits. It was found that the simplified model does predict the approximate asteroid directionality for spacecraft transfer orbits that are highly elliptical, such as minimum energy orbits to Jupiter or farther. However, the simplified model fails in two ways: (1) Most of the asteroids encountered early in the asteroid belt are near the perihelion of their orbit; whereas toward the outer edge of the belt, the asteroids are nearer their aphelion. Since the asteroids are not moving at their circular speed, the direction predicted by the simplified model may be in error by as much as 20°. (2) The distributions of asteroidal inclination and eccentricity will cause a spread in the directionality. Although this spread is small, it can cause the meteoroid flux on surfaces parallel to the direction of maximum flux to be nearly as high as the flux on a randomly tumbling surface.

The cometary flux is also directional, but because of uncertainties in the orbital distributions of cometary meteoroids, directionality is more difficult to predict than for the asteroids. However, most cometary meteoroids are in direct orbits around the Sun although their distributions of eccentricity and inclination have larger spreads than the asteroidal meteoroids. Thus, the same simplified model can be used to predict the approximate direction of cometary meteoroids, but the model would be valid only for highly elliptical spacecraft transfer orbits.

2.10 Uncertainties in the Model

Because data is scant for meteoroids in most of the mass range of interest in the asteroid belt and data interpretation unsure, exact uncertainties cannot be established. Models that are believed to have reasonable upper and lower limits have been developed. The assumptions used that probably contributed the largest uncertainties are examined below. The assumption that mass, velocity, and radial distributions are independent is not discussed but could lead to variation from actual conditions. The effect of possible clustering of meteoroids can be ignored in engineering design because clustering would reduce statistically the overall hazard to space vehicle missions. Experimenters, however, may have reason to take clustering into account when information is available.

2.10.1 Cometary Meteoroids

The cometary meteoroid environment in interplanetary space is probably better known than the asteroidal meteoroid environment since cometary meteoroids predominate near Earth and thus have been better observed with both satellite experiments and ground based observations. Satellite experiments have established the penetrating flux for cometary meteoroids in the mass range of approximately 10^{-9} to 10^{-6} gram on spacecraft in Earth orbit to within a factor of approximately 3.

The flux of larger meteoroids (masses approaching one gram) is estimated from the frequency of observed meteors in the Earth's atmosphere. The estimate of the meteoroid mass responsible for each observed meteor, however, can be in error as much as one order of magnitude too high or several orders of magnitude too low. However, a more likely range of uncertainty in mass is from a factor of 5 lower to a factor of 5 higher. This would lead to a factor of approximately 7 in uncertainty for the cometary flux near Earth. The free space cometary environment at 1 AU is not much greater than the uncertainty in the near-Earth environment. This is so because the gravitational factor applied to Earth-based observations for derivation of the free space cometary environment falls within fairly small uncertainty limits.

Various analyses lead to variations of particle population with distance from the Sun between R^0 and R^{-3}. If $R^{-1.5}$ is adopted as the nominal value and R^0 and R^{-3} are taken to be the extremes of possible radial distribution, an uncertainty factor of 4 results for the region between 0.4 and 2.5 AU. Combination of the uncertainty factor of 4 for radial distribution and the uncertainty factor of 7 for the cometary flux near Earth (derived from the mass uncertainty) gives an extreme uncertainty in cometary flux of 28 at 0.4 and 2.5 AU. This uncertainty lessens as the region of interest approaches 1 AU.

2.10.2 Asteroid Belt

The asteroid belt model population (as discussed earlier) is anchored at the large mass end by the observed asteroids and assumed to vary with mass as $m^{-\alpha}$. The validity of the assumption and the value of α probably constitute the largest uncertainties in the asteroidal meteoroid environment. An upper limit for the number of smaller asteroids is established by not allowing the number to be so great as to produce more reflected sunlight than is observed in the gegenschein (ref. 42). The value of α chosen in the model was not arbitrary but (as pointed out earlier) agreed with the steady-state mass distribution, based on collisions within the asteroid belt. It is also consistent with a limitation in particle mass to 10^{-9} gram and larger, based on the gegenschein. Steeper slopes than that selected for the model would lead to a particle cutoff at larger masses consistent with the gegenschein. Since no way exists to establish the proper cutoff, the extreme upper limit of the flux of particles greater than a given mass is just the value which would not produce reflections exceeding that of the gegenschein. The ratio of this upper limit to the model used (eq. 13a) is $26\ m^{0.17}$ ($m \geq 10^{-9}$ gram). Thus, if the asteroid mass is limited to particles of 10^{-9} gram or larger, the flux predicted from the model is essentially at the upper limit, whereas if asteroid mass is limited to 1 gram or larger, the limit of uncertainty could permit the actual flux to be higher than the flux predicted by the model by a factor of 26.

Additional uncertainty is introduced through the geometric particle albedo used in inferring a particle distribution to the gegenschein. Theoretically, geometric albedo may range from zero to infinity; however, the extremes of this range are never observed (sec. 2.7.1). A geometric albedo of approximately 0.1 is assumed to estimate the mass of the visual asteroids in the environment model. If the true albedo, however, is as low as 0.05, the assumption of 0.1 will lead to a mass too small by a factor of 3. If the true albedo is as high as 0.5, assumption of 0.1 will lead to a mass too large by a factor of 10. The upper limit flux for asteroidal meteoroids varies by a factor of +2 to −5 from the flux estimated with an albedo of 0.1 if it is assumed that the average albedos can vary from 0.05 to 0.5. The ratio of the upper limit to the model flux then becomes $52\ m^{0.17}$.

The lower limit of the meteoroid population in the asteroid belt is set by the cometary environment. If an extreme radial distribution of cometary particles is adopted which varies as R^{-3}, the ratio of the asteroid model environment to the cometary environment in the heart of the asteroid belt is $4.7 \times 10^3\ m^{0.37}$ ($m \geq 10^{-6}$). This expression implies that the meteoroid population in the asteroid belt could range from a factor of almost 30 lower than predicted by the asteroid model at $m = 10^{-6}$ gram to a factor of nearly 5000 lower for $m = 1$ gram.

2.10.3 The Outer Planets

The meteoroid environments of the outer planets ($R > 4.5$ AU) are probably totally cometary in origin. However, the validity of extrapolating the cometary environment into this region is complicated by the presence of the four larger planets. Each of these planets is capable of producing major perturbations in the meteoroid environment. The meteoroids observed on Earth are the results of an equilibrium state between these perturbations

(mostly by Jupiter) and the original distribution of meteoroid orbits. The relative balance of these two influences is not known.

2.10.4 Meteoroid Velocity

The uncertainty in the relative meteoroid velocity is not nearly as severe as the uncertainty in the mass distribution. Accurate measurements of meteoroid orbits through photographs of meteors, asteroids, and comets as well as the limitations of meteoroid velocity set by celestial mechanics, have reduced the uncertainty in relative meteoroid velocity. Uncertainties exist, however, mostly from selection effects. The average relative meteoroid velocity is probably uncertain by about ±25 percent for a spacecraft in near circular orbit around the Sun and only a few percent for spacecraft with very elliptical transfer orbits.

3. CRITERIA

A meteoroid environment for engineering applications to missions in interplanetary space and near a planet should be determined from the detailed models presented in section 3.1 or the simplified models presented in 3.2. The detailed models require numerical integration along the spacecraft trajectory, and the simplified model approximates the integral. Sample calculations for both the detailed and simplified models are given in appendix A.

3.1 Detailed Models

3.1.1 Cometary Meteoroids

3.1.1.1 Spatial Density and Flux Model

The spatial density of cometary meteoroids is expressed mathematically as follows:

$$\log_{10} S_c = -18.173 - 1.213 \log_{10} m - 1.5 \log_{10} R - 0.869 |\sin \beta| \qquad (26)$$

$$\text{for} \quad 10^{-6} \leq m \leq 10^{2}$$

$$\log_{10} S_c = -18.142 - 1.584 \log_{10} m - 0.063 (\log_{10} m)^2 - 1.5 \log_{10} R - 0.869 |\sin \beta| \qquad (27)$$

$$\text{for} \quad 10^{-12} \leq m \leq 10^{-6}$$

Spatial density is related to flux on a randomly tumbling surface by

$$F_c = \frac{1}{4} S_c \left(\overline{V_c^{-1}}\right)^{-1} \qquad (28)$$

where

S_c = number of cometary meteoroids of mass m or greater per cubic meter

m = mass of the meteoroid in grams

F_c = number of cometary meteoroids of mass m or greater per square meter per second

R = distance from the Sun in astronomical units (AU)

V_c = relative velocity of cometary meteoroids to the spacecraft in meters per second. (See section 3.1.1.3 for method of obtaining various weighted average velocities.)

β = heliocentric latitude

3.1.1.2 Mass Density

The mass density is assumed to be 0.5 g/cm^3 for all cometary meteoroids.

3.1.1.3 Relative Velocity

The average relative velocity of cometary meteoroids to a spacecraft is expressed as follows:

$$\overline{V}_c\,(R, \sigma, \theta) = R^{-1/2}\,\overline{U}_c\,(\sigma, \theta) \tag{29}$$

and the weighted average cometary velocity is found from

$$\left(\overline{V_c^{\,n}}\right)^{1/n} = \overline{V}_c\,\delta_c^{(n-1)/2} \tag{30}$$

where

$\overline{V}_c$ = average cometary velocity relative to the spacecraft, meters per second

R = distance from the Sun in astronomical units (AU)

$\overline{U}_c$ = cometary velocity parameter, given in figure 2 as a function of σ and θ, 10^3 meters AU$^{1/2}$/sec

σ = ratio of the spacecraft's heliocentric speed at R to the speed required for a circular orbit of radius R

θ = angle between the spacecraft velocity vector and the surface of an imaginary sphere of radius R in degrees

δ_c = velocity weighting parameter, expressed as a function of σ and θ in figure 3

Values for $\overline{U}_c$ can also be found from the expression

$$\overline{U}_c = 31.29 \times 10^3 (1.30 - 1.9235 \sigma \cos\theta + \sigma^2)^{1/2} \quad (31)$$

3.1.1.4 Directionality

For most types of spacecraft transfer orbits, cometary meteoroids may be considered omnidirectional; thus, the flux on any part of an oriented spacecraft is considered to be the same as the flux on the surfaces of a randomly tumbling spacecraft.

3.1.2 Asteroidal Meteoroids

3.1.2.1 Spatial Density and Flux Model

The spatial density of asteroidal meteoroids is expressed mathematically as follows:

$$*\log_{10} S_a = -15.79 - 0.84 \log_{10} m + f(R) + g(R) \cos\lambda + h(\beta) \quad (32)$$

$$\text{for} \quad 10^{-9} \leq m \leq 10^2$$

$$\log_{10} S_a = -8.23 + f(R) + g(R) \cos\lambda + h(\beta) \quad (33)$$

$$\text{for} \quad 10^{-12} \leq m \leq 10^{-9}$$

Spatial density is related to flux on a randomly tumbling surface by

$$F_a = \frac{1}{4} S_a \left(\overline{V_a^{-1}}\right)^{-1} \quad (34)$$

*This equation may be extended to 10^{19} grams although such large asteroids are not usually of interest to spacecraft designers.

where

S_a = number of asteroidal meteoroids of mass m or greater per cubic meter

m = mass of the meteoroid in grams

F_a = number of asteroidal meteoroids of mass m or greater per square meter per second

R = distance from the Sun in astronomical units, AU

$f(R) = \log_{10} [S(R)/S(R = 2.5)]$ (values are given in fig. 8)

g(R) = coefficient of $\cos \lambda$. (values are given in fig. 7)

λ = heliocentric longitude of the spacecraft

$h(\beta) = \log_{10} [S(\beta)/S(\beta = 0)]$ (Values are given in fig 9)

β = heliocentric latitude

V_a = relative velocity of asteroidal meteoroids to the spacecraft in meters per second. (See sec. 3.1.2.3 for method of obtaining various weighted average velocities.)

3.1.2.2 Mass Density

The mass density is assumed to be 3.5 g/cm^3 for all asteroidal meteoroids.

3.1.2.3 Relative Velocity

The average relative velocity of asteroidal meteoroids is

$$\bar{V}_a (R, \sigma, \theta) = R^{-1/2} \bar{U}_a (R, \sigma, \theta) \tag{35}$$

and the weighted average asteroidal velocity is found from

$$\left(\overline{V_a^n}\right)^{1/n} = \bar{V}_a \tag{36}$$

where

$\bar{V}_a$ = average asteroidal velocity relative to the spacecraft

R = distance from the Sun in astronomical units (AU)

$\bar{U}_a$ = asteroidal velocity parameter, given in figures 10, 11, and 12 for R = 1.7, 2.5, and 4.0, respectively, as a function of σ and θ, 10^3 meters $AU^{1/2}$/sec (For distances from the Sun other than those given, $\bar{U}_a$ is found by linear interpolation or extrapolation.)

σ = ratio of the spacecraft's heliocentric speed at R to the speed required for a circular orbit of radius R

θ = angle between the spacecraft velocity vector and the surface of an imaginary sphere of radius R in degrees

Values for $\bar{U}_a$ can also be found from the following expressions:

Figure 10 with R = 1.7 AU,

$$\bar{U}_a = 30.05 \times 10^3 (1.2292 - 2.1334 \sigma \cos\theta + \sigma^2)^{1/2} \quad (37)$$

Figure 11 with R = 2.5 AU,

$$\bar{U}_a = 29.84 \times 10^3 (1.0391 - 1.9887 \sigma \cos\theta + \sigma^2)^{1/2} \quad (38)$$

Figure 12 with R = 4.0 AU,

$$\bar{U}_a = 29.93 \times 10^3 (0.9593 - 1.923 \sigma \cos\theta + \sigma^2)^{1/2} \quad (39)$$

3.1.2.4 Directionality

Since asteroids are in near circular orbits around the Sun, they may be considered nearly monodirectional relative to the spacecraft for most types of spacecraft orbits. The approximate direction of the asteroids relative to the spacecraft can be predicted by the vector relationship between the spacecraft velocity vector and a circular orbit velocity vector. This approximation breaks down as the spacecraft velocity vector approaches a circular orbit; that is, as a zero relative velocity is approached by this procedure, the asteroids become more omnidirectional.

A surface whose normal vector is pointing in the direction of a truly monodirectional flux will encounter exactly 4 times the flux on a randomly tumbling surface. If it is pointed 60° from this direction, the surface will encounter exactly the same flux as the randomly tumbling surface. Orbits of the asteroids are sufficiently noncircular to reduce the flux in the direction of maximum flux to about 3 times the flux on a randomly tumbling surface; the flux 90° away from this direction will be approximately the same as on the randomly tumbling surface.

3.2 Simplified Model

To use the model given in section 3.1, it is necessary to numerically integrate along the trajectory of the spacecraft, as in the sample calculations given in appendix A.1. However after examination of several trajectories in the ecliptic plane, including some extreme ones, it was found that this integration can be approximated to give the total number of meteoroid impacts to within about 50 percent for most types of trajectories. The following model represents such an approximation and is presented to give the designer a "quick-look" at the meteoroid hazard.

3.2.1 Cometary Meteoroids

The average cometary flux on a spacecraft between two points of a transfer orbit can be approximated by taking the geometric average of the flux at the beginning and end points of the trajectory. For a first approximation, the weighted average velocity can be approximated by the average velocity, and from figure 2, the average cometary velocity can be approximated by

$$V_c = 2(1 + 0.8\,\theta_r) \times 10^4\, R^{-1/2} \tag{40}$$

where V_c is in meters/sec, R is the distance from the Sun in AU, and θ_r is defined as in figure 2 but expressed in radians. The flux at R_1 and R_2 is then approximated using equations 26 and 27 with 28 and 40 (approximating $(\overline{V_c^{-1}})^{-1}$ with V_c in equation 40). The geometric average of the two fluxes is taken (which is the same as averaging their logarithms) to give the average cometary flux between R_1 and R_2 as

$$\log \bar{F}_c = -14.47 - 1.213 \log m - 1.0 \log R_1 R_2 + \frac{1}{2} \log \left[1 + 0.8\,\theta_r(R_1)\right]\left[1 + 0.8\,\theta_r(R_2)\right] \tag{41}$$

$$\text{for} \quad 10^{-6} \leq m \leq 10^{2}$$

$$\log \bar{F}_c = -14.44 - 1.584 \log m - 0.063 (\log m)^2 - 1.0 \log R_1 R_2 + \frac{1}{2} \log \left[1 + 0.8\,\theta_r(R_1)\right]\left[1 + 0.8\,\theta_r(R_2)\right] \tag{42}$$

$$\text{for} \quad 10^{-12} \leq m \leq 10^{-6}$$

where

$\bar{F}_c$ = average number of cometary meteoroids of mass m or greater per square meter per second between R_1 and R_2

m = meteoroid mass in grams

R_1 = nearest approach to the Sun of the spacecraft in AU

R_2 = largest distance to the Sun of the spacecraft in AU

θ_r (R) = angle between the spacecraft velocity vector at R and the surface of an imaginary sphere of radius R in radians

Thus, the total number of cometary impacts between R_1 and R_2 is

$$N_c = \bar{F}_c A t \tag{43}$$

where A is the surface area of the spacecraft in square meters and t is the time in seconds to travel from R_1 to R_2.

The cometary velocity averaged over the spacecraft trajectory is approximately the same as the velocity at R_1, or

$$V_{cm} = 2\left[1 + 0.8\,\theta_r (R_1)\right] \times 10^4\, R_1^{-1/2} \tag{44}$$

where V_{cm} is in meters/sec.

3.2.2 Asteroidal Meteoroids

The average asteroidal flux between two points of a transfer orbit can be approximated by taking the arithmetical or regular average of the flux between certain points of the trajectory. From figures 10, 11, and 12, the average asteroidal velocity can be approximated by

$$V_a = (1 + 2\,\theta_r) \times 10^4\, R^{-1/2} \tag{45}$$

where θ_r is expressed in radians.

The asteroidal flux at R is approximated by combining equations 32 and 33 with 34 and 45 (approximating $(\overline{V_a^{-1}})^{-1}$ with V_a in equation 45) to obtain

$$\log F_a = -12.39 - 0.84 \log m + f(R) + g(R) \cos \lambda - \frac{1}{2} \log R + \log \left[1 + 2\theta_r (R)\right] \quad (46)$$

$$\text{for} \quad 10^{-9} \leq m \leq 10^{2}$$

$$\log F_a = -4.83 + f(R) + g(R) \cos \lambda - \frac{1}{2} \log R + \log \left[1 + 2\theta_r (R)\right] \quad (46a)$$

$$\text{for} \quad 10^{-12} \leq m \leq 10^{-9}$$

where

F_a = flux at R of asteroids of mass m or greater, per square meter-sec.

m = asteroidal mass in grams.

f(R) = $\log_{10}$ of the ratio of the spatial density at R to the spatial density at R = 2.5 (values are given in fig. 8)

R = distance from the Sun in AU

g(R) = coefficient of cos λ (values are given in fig. 7)

λ = heliocentric longitude of the spacecraft

θ_r = angle between the spacecraft velocity vector at R and the surface of an imaginary sphere of radius R in radians

V_a = average asteroidal velocity at R in meters/sec

Outside the range of 1.7 to 4.0 AU, the asteroid flux is small enough to be ignored as a hazard to spacecraft. Within this region, the average flux is found by dividing the belt into the following two regions: 1.7 to 2.5 AU, and 2.5 to 4.0 AU. The average flux in each region is then the average of the flux at the beginning and end points of the trajectory in each region. That is,

$$(\overline{F}_a)_{1,2} = \frac{F(R_1) + F(R_2)}{2} \quad (47)$$

$$1.7 \text{ AU} \leq R_1 \leq R_2 \leq 2.5 \text{ AU}$$

and

$$(\bar{F}_a)_{3,4} = \frac{F(R_3) + F(R_4)}{2} \tag{48}$$

$$2.5 \text{ AU} \leq R_3 \leq R_4 \leq 4.0 \text{ AU}$$

where

$(\bar{F}_a)_{1,2}$ = the average asteroidal flux in the region 1.7 AU to 2.5 AU

$(\bar{F}_a)_{3,4}$ = the average asteroidal flux in the region 2.5 AU to 4.0 AU

The total number of impacts on the spacecraft is then

$$N_a = \left[(\bar{F}_a)_{1,2}\, t_{1,2} + (\bar{F}_a)_{3,4}\, t_{3,4}\right] A \tag{49}$$

where

$t_{1,2}$ = time for the spacecraft to go from R_1 to R_2 in seconds

$t_{3,4}$ = time for the spacecraft to go from R_3 to R_4 in seconds

A = surface area of spacecraft in square meters

The average asteroidal velocity for a mission in general is difficult to approximate but will be nearly the same average relative velocity found when the spacecraft is at a distance from the Sun corresponding to the maximum asteroidal spatial density.

For missions to the outer planets which go completely through the asteroid belt, the total number of asteroid impacts is nearly independent of the spacecraft transfer orbit. The number of impacts per square meter of surface area is given by

$$\log_{10} (N_a/A) = -5.0 - 0.84 \log_{10} m \tag{50}$$

and the average asteroidal velocity for such a mission is about the same as the relative velocity when R = 2.5 AU.

3.3 Modification in Environment Near a Planet

Abnormalities, peculiar to particular planets, are given in individual design criteria monographs about those planets. The secondary meteoroid environment induced by impacts on the lunar surface is given in reference 1. The meteoroid environments suggested by the irregular satellites of the major planets, particularly Jupiter, and by Saturn's rings may be of concern for flights near those planets. Monographs on Jupiter and Saturn are to be published in coming months.

3.3.1 Flux Near a Planet

The following procedure is used to determine the meteoroid environment near a planet.

The environment at various distances from the Sun is found using section 3.1. The decrease in meteoroid flux which results from planetary shielding is obtained by the factor

$$\eta = \frac{1}{2} + \frac{1}{2}\left(1 - r_p^2/r^2\right)^{1/2} \tag{51}$$

and the increase in meteoroid flux which results from the gravitational effect of a planet is obtained by the factor

$$G = 1 + 0.76\,\frac{RV_p^2\, r_p}{V_e^2\, r} \tag{52}$$

where

η = planetary shielding factor

G = gravitational increase in flux factor

r_p = radius of the planet

r = distance from the planet's center (same units as r_p)

R = distance of the planet from the Sun in astronomical units

V_e = escape velocity from the Earth's surface

V_p = escape velocity from the planet's surface (same units as V_e)

Escape velocities for the planets are given in table 1.

3.3.2 Velocity Near a Planet

The average relative velocities near the planets Mercury, Venus, Earth, and Mars are increased by less than 3 percent.

For the large planets, however, the planet's escape velocity must be used as the average meteoroid velocity relative to the planet. The average velocity relative to a spacecraft near the large planets is found by

$$\bar{V} = \sqrt{\frac{r_p V_p^2}{r} + V_s^2} \tag{53}$$

where

$\bar{V}$ = average relative velocity of a spacecraft near a large planet (meters/sec)

r_p = radius of planet

r = distance of the spacecraft from planet (same units as r_p)

V_p = escape velocity from planet's surface (meters/sec)

V_s = velocity of spacecraft relative to the planet (meters/sec)

TABLE 1

ESCAPE VELOCITIES FROM THE SURFACE OF THE PLANETS

Planet	Average distance from Sun (AU)	V_p (meters/sec)	$0.76 RV_p^2/V_e^2$ (eq. 52)
Mercury	0.39	4.3×10^3	0.04
Venus	.72	10.4×10^3	.47
Earth	1.00	11.2×10^3	.76
Mars	1.52	5.1×10^3	.24
Jupiter	5.20	61.0×10^3	117.23
Saturn	9.54	36.7×10^3	77.85
Uranus	19.19	22.4×10^3	58.34
Neptune	30.07	25.6×10^3	119.40

REFERENCES

1. Anon: Meteoroid Environment Model - 1969 (Near Earth to Lunar Surface). NASA SP-8013, Mar. 1969.

2. Lovell, A. C.: Meteor Astronomy. Oxford Univ. Press, 1954.

3. McKinley, D. W.: Meteor Science and Engineering. McGraw-Hill Book Company, Inc., 1961.

4. Watson, F. G.: Between the Planets. Harvard University Press, 1956.

5. Alexander, W. M.; McCracken, C. W.; Secretan, L.; and Berg, O.: Review of Direct Measurements of Interplanetary Dust from Satellites and Probes. Space Research III, Proceedings of the Third International Space Science Symposium, Washington, D. C., May 2-5, 1962. John Wiley & Sons, pp. 891-917.

6. Middlehurst, B. M.; and Kuiper, G. P.; editors: The Moon, Meteorites, and Comets. Vol. IV of the Solar System. Chicago Univ. Press, 1963.

7. Hastings, E. C.: The Explorer XVI Micrometeoroid Satellite. Supplement III, Preliminary Results for Period May 27, 1963, through July 22, 1963. NASA TM X-949, Mar. 1964.

8. O'Neal, R. L.: The Explorer XXIII Micrometeoroid Satellite. NASA TN D-4284, June 1968.

9. Alexander, W. M.; McCracken, C. W.; and Bohn, J. L.: Zodiacal Dust-Measurements by Mariner IV. Science, vol. 149, no. 3689, September 10, 1965, pp. 1240-1241.

10. Clifton, K. S.; and Naumann, R. J.: Pegasus Satellite Measurements of Meteoroid Penetration. NASA TM X-1316, Dec. 1966.

11. Hawkins, G. S.; and Upton, E. K.: The Influx Rate of Meteors in the Earth's Atmosphere. Astrophys. J., vol. 128, 1958, pp. 727-735.

12. Whipple, F. L.: The Meteoritic Environment of the Moon. Proc. Roy. Soc. (London), series A, vol. 296, Feb. 7, 1967, pp. 304-315.

13. Lindblad, B. A.: The Luminosity Function of Sporadic Meteors and the Extrapolation of the Meteor Influx Rate to the Micrometeorite Region. The Proceedings of a Symposium on Meteor Orbits and Dust, NASA SP-135, 1967, pp. 171-180.

14. McCrosky, R. E.; and Ceplecha, Z.: Photographic Network for Fireballs, Smithsonian Astrophysical Observatory Special Report 288, Oct. 4, 1968.

15. Elford, W. G.: The Incidence of Meteors on the Earth Derived from Radio Observations. The Proceedings of a Symposium on Meteor Orbits and Dust, NASA SP-135, 1967, pp. 121-132.

16. Nilsson, C. S.; and Southworth, R. B.: The Flux of Meteors and Micrometeoroids in the Neighborhood of the Earth. Smithsonian Astrophysical Observatory Special Report No. 263, December 1967.

17. Kashcheyev, B. L.; and Lebedinets, V. N.: Radar Studies of Meteors. The Proceedings of a Symposium on Meteor Orbits and Dust, NASA SP-135, 1967, pp. 183-199.

18. Southworth, R. B.: Phase Function of the Zodiacal Cloud. Smithsonian Astrophysical Observatory Special Report 239, May 31, 1967.

19. Van de Hulst, H. C.: Zodiacal Light in the Solar Corona. Astrophys. J. vol. 105, no. 3, Jan.-May 1947, pp. 471-488.

20. Beard, David B.: Interplanetary Dust Distribution. Astrophys. J. vol. 129, no. 2, Jan.-May 1959, pp. 496-506.

21. Ingham, M. F.: Interplanetary Matter. Space Science Reviews, vol. 1, no. 3, 1962, pp. 576-588.

22. Giese, R. H.: Light Scattering by Small Particles and Models of Interplanetary Matter Derived from the Zodiacal Light. Space Science Reviews, vol. 1, no. 2, 1962, pp. 589-611.

23. Weinberg, J. L., editor. The Zodiacal Light and the Interplanetary Medium. A Symposium held at East-West Center, University of Hawaii, Honolulu, Hawaii, Jan. 30-Feb. 2, 1967. NASA SP-150.

24. Naumann, R. J.: The Near-Earth Meteoroid Environment, NASA TN D-3717, Nov. 1966.

25. Zook, Herbert A.; and Kessler, Donald J.: The Zodiacal Light and Meteoroid Measurements. Trans. AGU, vol. 49, no. 1, Mar. 1968, pp. 244-245.

26. Makover, S. G., editor: Ephemerides of Minor Planets for 1967. Published by the Inst. of Theoret. Astron. of the Acad. of Sci. USSR, Science Pub. House, Moscow, 1966.

27. Kuiper, G. P.; Fujita, Y.; Gehrels, T.; Groeneveld, I.; Kent, J.; Van Biesbroeck, G.; and Van Houten, C. J.: Survey of Asteroids. Astrophys. J. Supplement Series, Suppl. 32, vol. IIIm, 1958, pp. 289-335.

28. Hawkins, G. S.: Interplanetary Debris Near the Earth. The Annual Review of Astronomy and Astrophysics, Leo Goldberg, editor. George Banta Co., Inc., 1964, vol. 2, pp. 149-164.

29. Brown, Harrison: The Density and Mass Distribution of Meteoritic Bodies in the Neighborhood of the Earth's Orbit. J. of Geophys. Res. vol. 65, no. 6, June 1960, pp. 1679-1683.

30. McCrosky, R. E.; and Boeschenstein, H.: The Prairie Meteorite Network. Smithsonian Astrophysical Observatory Special Report no. 173, May 1965.

31. McCrosky, R. E.: The Lost City Meteorite Fall. Sky and Telescope, vol. 39, no. 3, March 1970, pp. 154-158.

32. Ceplecha, Z.: Multiple Fall of Pribram Meteorites Photographed. Double-station photographs of the fireball and their relations to the found meteorites. Bull. Astron, Inst. Czechoslovakia, vol. 12, 1961, pp. 21-47.

33. Wetherill, G. W.; and Williams, J. G.: Evaluation of the Apollo Asteroids as Sources of Stone Meteorites. J. of Geophys. Res. vol. 73, no. 2, Jan. 15, 1968, pp. 635-648.

34. Baldwin, Ralph B.: Lunar Crater Counts, The Astronom. J. vol. 69, no. 5, June 1964, pp. 377-392.

35. Hartmann, William K.: Secular Changes in Meteoritic Flux Through the History of the Solar System. Icarus, vol. 4, no. 2, May 1965, pp. 207-213.

36. Hartmann, William K.: Lunar Crater Counts - VI: The Young Craters Tycho, Aristorchus, and Copernicus. Communications of the Lunar and Planetary Lab., Univ. of Arizona Press, vol. 7, nos. 114-122, pp. 145-156.

37. Marcus, A. H.: A Stochastic Model for the Formation and Survival of Lunar Craters. Icarus, vol. 5, 1966, pp. 165-200.

38. Marcus, A. H.: Number Density of Martian Craters. Bellcomm Report TR-68-710-1, Jan. 29, 1968.

39. Piotrowski, S.: Collisions of Asteroids. Acta Astronomica, vol. 5, Oct. 1953, pp. 115-138.

40. Hawkins, Gerald S.: Asteroidal Fragments. The Astronom. J., vol. 65, no. 5, June 1960, pp. 318-322.

41. Dohnanyi, J. S.: Collisional Model of Asteroids and their Debris. J. Geophys. Res., vol. 74, no. 10, May 15, 1969, pp. 2531-2554.

42. Kessler, Donald J.: Upper Limit on the Spatial Density of Asteroidal Debris. AIAA Journal, vol. 6, no. 12, Dec. 1968, p. 2450.

43. McCrosky, R. E.; and Posen, A.: Orbital Elements of Photographic Meteors. Smithsonian Contributions to Astrophysics 4, no. 2, 1961.

44. Hawkins, G. S.; and Southworth, R. B.: The Statistics of Meteors in the Earth's Atmosphere. Smithsonian Contributions to Astrophysics 2, 1958, pp. 349-364.

45. Dohnanyi, J. S.: Model Distribution of Photographic Meteors. Bellcomm Inc. Report TR-66-340-1, 1966.

46. Kessler, D. J.: Average Relative Velocity of Sporadic Meteors in Interplanetary Space. AIAA Journal, vol. 7, no. 12, Dec. 1969, pp. 2337-2338.

47. Dalton, C. C.: Statistical Analysis of Photographic Meteor Data, Part II: Verniani's Luminous Efficiency and Supplemented Whipple Weighting. NASA TN X-53360, Nov. 1965.

48. Whipple, F. L.: On Meteoroids and Penetration. J. Geophys. Res., vol. 68, no. 17, 1963, pp. 4929-4939.

49. Burbank, P. B.; Cour-Palais, B. G.; and McAllum, W. E.: A Meteoroid Environment for Near-Earth, Cislunar, and Near-Lunar Operations. NASA TN D-2747, Apr. 1965.

50. Wetherill, G. W.: Collisions in the Asteroid Belt. J. Geophys. Res., vol. 72, no. 9, May 1, 1967, pp. 2429-2444.

51. Whipple, F. L.: The Meteoritic Risk to Space Vehicles, Vistas in Astronautics, Pergammon Press, Los Angeles, 1958.

52. Verniani, F.: On the Luminous Efficiency of Meteors, Research in Space Sciences. Smithsonian Astrophysical Observatory, Special Report No. 145, 1964.

53. Verniani, F.: II Nuovo Cimento, vol. 33, no. 4, Aug. 1964, pp. 4453-4464.

54. Ceplecha, Z.: Classification of Meteor Orbits. The Proceedings of a Symposium on Meteor Orbits and Dust, NASA SP-135, 1967, pp. 35-65.

55. Whipple, Fred L.: On Maintaining the Meteoritic Complex. Smithsonian Astrophysical Observatory, Special Report 239, May 31, 1967, SP-150, pp. 409-426.

56. Jacchia, Luigi; and Whipple, Fred L.: Precision Orbits of 413 Photographic Meteors. Smithsonian Contributions to Astrophysics, vol. 4, no. 4 (1961) pp. 97-129.

57. Briggs, Robert E.: Steady-State Space Distribution of the Meteoric Particles under the Operation of the Poynting - Robertson Effect. Astronom. J., 67, no. 10, 1962, Dec. no. 1305, pp. 710-723.

58. Southworth, Richard B.: Space Density of Radio Meteors. Smithsonian Astrophysical Observatory, Special Report, May 31, 1967.

59. Narin, Francis: Spatial Distribution and Motion of the Known Asteroids. J. of Spacecraft and Rockets, vol. 3, no. 9, Sept. 1966, pp. 1438-1440.

60. Kessler, D. J.: Spatial Density of the Known Asteroids in the Ecliptic Plane. NASA TM X-58026, Mar. 1969.

61. Öpik, E. J.: Collision Probabilities with the Planets and the Distribution of Interplanetary Matter. Proc. of the Roy. Irish Acad., vol. 54, sec. A, Apr. 1951, pp. 165-199.

62. Dycus, R. D.; Bradford, D. C.; and Luebbe, R. C.: On the Meteoroid Flux in Cislunar Space. R.A.S.C. Journal, vol. 59, no. 4, Aug. 1965, pp. 161-172.

63. Divari, N. B.: Zodiacal Light. Soviet Physics Uspekhi, vol. 7, no. 5, pp. 681-695, March-April 1965.

64. Kresak, L.: The Asymmetry of the Asteroid Belt. Astronomical Institutes of Czechoslavakia, Bull., vol. 18, no. 1, 1967, pp. 27-36.

65. Allen, Clabon Walter: Astrophysical Quantities, Univ. of London, Athlone Press, Distributed in USA by Oxford Univ. Press, New York, 2nd. ed., 1963.

66. Southworth, Richard B.: The Size Distribution of the Zodiacal Particles. Annals of the New York Acad. of Sciences, vol. 119, article 1, Nov. 11, 1964, pp. 54-67.

67. Kuiper, G. P.: The Origin of the Satellites and the Trojans. Vistas in Astronomy, Arthur Beer, ed. 1956, Vol. 2, Pergamon Press, pp. 1631-1666.

APPENDIX A

SAMPLE APPLICATIONS OF THE INTERPLANETARY METEOROID MODELS

As examples for applying the interplanetary meteoroid models in section 3, a typical trajectory for a Jupiter flyby mission is used. Such a trajectory could have the following characteristics:

Date of Earth departure	2441380 (Julian date, days)
Date of Jupiter arrival	2441980 (Julian date, days)
Semi-major axis	3.736 AU
Eccentricity	0.735
Inclination to the ecliptic	1.55°
Distance from Sun at encounter	5.07 AU

A.1 Detailed Model (Numerical Integration Along Trajectory)

The position and velocity as a function of time of the spacecraft can be found through the following standard equations:

$$T = \frac{a^{3/2}}{2\pi} (E - e \sin E) \tag{A1}$$

$$R = a(1 - e \cos E) \tag{A2}$$

$$\cos \upsilon = \frac{\cos E - e}{1 - e \cos E} \tag{A3}$$

$$\sigma = (2 - R/a)^{1/2} \tag{A4}$$

$$\cos\theta = \left[\frac{a(1 - e^2)}{R(2 - R/a)}\right]^{1/2} \tag{A5}$$

$$\lambda = \upsilon + \bar{\omega} \tag{A6}$$

where

T = time since perihelion passage in years

E = eccentric anomaly

e = eccentricity

a = semi-major axis in AU

R = distance from the Sun in AU

υ = true anomaly

σ = ratio of spacecraft speed to the speed of a circular orbit

θ = angle between spacecraft velocity vector and the surface of an imaginary sphere of radius R

λ = heliocentric longitude

$\bar{\omega}$ = longitude of perihelion

The heliocentric latitude, β, need not be calculated for this example. An orbital inclination of 1.55° means that the maximum β that the spacecraft will have is also 1.55°, and the spacecraft will spend only a small amount of time even this far from the ecliptic. Since the spatial density of meteoroids varies very little with β when β is this close to the ecliptic plane, a value of $\beta = 0$ can be used for the entire mission.

Since the transfer orbit is very close (less than 3°) to perihelion at launch, the perihelion passage date will be approximately the Julian date of 2441380 (March 3, 1972) where $\omega \cong 163°$. From the first two equations, the time from perihelion passage can be calculated as a function of R. The orbit is then approximated as a series of step functions by placing the spacecraft at a particular R for time dt. At each R, values for σ, θ, and λ are

computed. The total number of impacts for the mission can be numerically integrated from

$$N_a = A \int F_a \, dt \tag{A7}$$

$$N_c = A \int F_c \, dt \tag{A8}$$

$$N_t = N_a + N_c \tag{A9}$$

The average velocity for the mission can be found from

$$\overline{V_{am}^n} = \int F_a \, \overline{V_a^n} \, dt \Big/ \int F_a \, dt \tag{A10}$$

$$\overline{V_{cm}^n} = \int F_c \, \overline{V_c^n} \, dt \Big/ \int F_c \, dt \tag{A11}$$

$$\overline{V_t^n} = \frac{N_a \, \overline{V_{am}^n} + N_c \, \overline{V_{cm}^n}}{N_a + N_c} \tag{A12}$$

where the limits of integration are the beginning and end of the space mission (i.e., in this case, from time of Earth launch to Jupiter flyby) and

N_a = total number of asteroidal impacts for the mission

A = surface area of spacecraft in square meters

F_a = flux of asteroidal meteoroids at R

dt = time interval that spacecraft is exposed to flux

N_c = total number of cometary impacts for the mission

F_c = flux of cometary meteoroids at R

N_t = total number of meteoroid impacts for the mission

$\overline{V_{am}^n}$ = weighted average asteroidal velocity for the mission

$\overline{V_a^n}$ = weighted average asteroidal velocity at R

$\overline{V_{cm}^n}$ = weighted average cometary velocity for the mission

$\overline{V_c^n}$ = weighted average cometary velocity at R

$\overline{V_t^n}$ = weighted average meteoroid velocity for the mission.

The proper weighted average velocity (i.e., the value of n) will depend on the type of transformation being made; for example, from flux as a function of mass to flux as a function of energy, momentum, or penetration thickness. If

$$F = A\, m^{-\alpha} \tag{A13}$$

where A is a constant and if $d = Bm^{\gamma}V^{\epsilon}$, then flux as a function of the parameter d is expressed by

$$F = AB^{\alpha/\gamma}\overline{V^{\alpha\epsilon/\gamma}}\, d^{-\alpha/\gamma} \tag{A14}$$

where B, γ, and ϵ are constants. Thus

$$n = \alpha\, \epsilon/\gamma \tag{A15}$$

A value of n = 1.0 is used in the analysis presented in table A-1.

In table A-1, column (1) is the spacecraft distance from the Sun, and column (2) is the time spent at that distance (i.e., the time to go from $R - \Delta R$ to $R + \Delta R$); these two parameters follow from equations (A1) and (A2). Column (3) follows from equations (A3) and (A6), and columns (4) and (5) from equations (A5) and (A4), respectively. Columns (6) through (9) and (12) through (16) follow from section 3.1. A mass of 10^{-3} gram was arbitrarily assumed. As will be shown, once the analysis is complete for this mass size, other mass sizes can quickly be considered.

From the sums of columns (10) and (17) the total number of cometary and asteroidal impacts is 1.71×10^{-4}/ square meter and 2.46×10^{-3}/square meter, respectively. These sums

TABLE A-1

METEOROID IMPACTS OF MASS 10^{-3} GRAM AND LARGER FOR A JUPITER FLYBY MISSION

1	2	3	4	5	6	7	8	9	10	11
R in AU	Δt, 8.64×10^4 sec (days)	λ, deg	θ, deg	σ	δ_c	S_c, 10^{-15}/cubic meter	$\bar{V}_c$, 10^3 meter/sec	F_c, 10^{-12}/square meter sec	$F_c \Delta t$, 10^{-6}/square meters	$F_c \Delta t \bar{V}_c$, 10^{-6} km/square meters - sec
1.04	32.2	—	11.6	1.31	1.33	2.73	22.7	11.6	32.4	735
1.14	13.4	—	19.2	1.30	1.28	2.38	23.2	10.8	12.5	290
1.23	9.6	—	23.9	1.29	1.26	2.14	23.5	10.0	8.3	194
1.31	10.3	—	27.0	1.28	1.24	1.93	23.6	9.2	8.2	193
1.41	11.0	—	29.8	1.27	1.22	1.74	23.5	8.4	8.0	187
1.51	11.9	242	32.5	1.26	1.20	1.57	23.4	7.7	7.9	184
1.63	12.8	249	34.8	1.25	1.19	1.42	23.1	6.9	7.6	176
1.76	13.8	255	37.0	1.24	1.18	1.23	22.8	5.9	7.1	162
1.90	14.9	260	38.9	1.22	1.17	1.11	22.3	5.3	6.8	152
2.05	16.0	266	40.6	1.21	1.16	1.00	21.8	4.7	6.5	142
2.20	17.3	270	41.9	1.19	1.15	.90	21.2	4.1	6.2	131
2.36	18.5	275	43.1	1.17	1.15	.81	20.6	3.6	5.8	119
2.53	19.9	—	44.2	1.15	1.15	.73	20.0	3.2	5.5	109
2.71	21.2	—	45.1	1.13	1.14	.66	19.4	2.8	5.1	100
2.89	22.6	—	45.9	1.11	1.14	.60	18.8	2.5	4.8	91
3.07	24.1	—	46.4	1.09	1.14	.54	18.2	2.2	4.5	82
3.26	25.6	—	46.9	1.06	1.13	.50	17.6	1.9	4.3	76
3.45	27.1	—	47.1	1.04	1.13	.45	17.0	1.7	4.0	67
3.64	28.6	—	47.2	1.01	1.13	.42	16.4	1.5	3.8	62
3.83	30.1	—	47.2	0.99	1.13	.39	15.9	1.4	3.6	57
4.02	31.6	—	47.1	0.96	1.13	.37	15.3	1.3	3.4	52
4.21	33.1	—	46.9	0.93	1.12	.34	14.8	1.1	3.2	48
4.40	34.5	—	46.4	0.91	1.12	.32	14.3	1.0	3.0	44
4.58	36.0	—	45.9	0.88	1.12	.30	13.8	.9	2.9	40
4.76	37.4	—	45.1	0.85	1.12	.28	13.4	.8	2.7	36
5.0	48.7	—	44.2	0.82	1.12	.26	12.8	.7	3.1	40
SUM:									171.2	3570

TABLE A-1 (Continued)

12	13	14	15	16	17	18
g(R) cos λ	f(R)	S_a, 10^{-15}/cubic meter	$\bar{V}_a$, 10^3 meter/sec	F_a, 10^{-12}/square meter sec	$F_a \Delta t$, 10^{-6} square meter	$F_a \Delta t \bar{V}_a$, 10^{-6} km/square meter sec
–	–	–	–	–	–	–
–	–	–	–	–	–	–
–	–	–	–	–	–	–
–	–	–	–	–	–	–
–	–	–	–	–	–	–
- .01	-2.22	.32	18.1	1.45	1.49	26.9
- .06	-1.84	.68	18.3	3.11	3.44	63.0
- .13	-1.28	2.19	18.4	10.07	12.01	221.
- .09	-0.81	6.75	18.2	30.7	39.5	720.
- .02	-0.42	19.50	17.7	86.3	119.3	2111.
0.00	-0.13	39.98	17.1	171.	255.	4343.
0.00	-0.02	51.30	16.7	214.	342.	5717.
–	-0.0	53.70	16.2	217.	374.	6058.
–	-0.05	47.8	15.7	188.	344.	5395.
–	-0.12	40.7	15.2	155.	302.	4590.
–	-0.21	33.1	14.7	122.	253.	3723.
–	-0.34	24.5	14.1	86.4	191.	2693.
–	-0.55	15.1	13.6	51.3	120.	1635.
–	-0.84	7.76	12.9	25.0	61.8	798.
–	-1.23	3.16	12.3	9.72	25.3	311.
–	-1.64	1.23	11.9	3.66	9.99	119.
–	-2.12*	.41	11.5	1.18	3.37	38.8
–	-2.65	.12	11.0	.33	.98	10.8
–	–	–	–	–	–	–
–	–	–	–	–	–	–
–	–	–	–	–	–	–
SUM:					2458.	38574.

are divided into the sums of columns (11) and (18), respectively, to give the average cometary and asteroidal impact velocities for the mission at 20.9 km/sec and 15.7 km/sec, respectively. The total number of impacts of mass 10^{-3} gram or larger for the mission is 3.31 x 10^{-3}/square meter at an average velocity of 16.0 km/sec. Thus, if the spacecraft had 10 square meters of surface area, it would be hit by 2.63 x 10^{-2} particles of mass equal to or greater than 10^{-3} gram at an average velocity of 16.0 km/sec.

To obtain flux and velocity with other assumed masses, factors can be developed to use with the results determined above for m = 10^{-3} gram.

From figures 1 and 6 or equations 26-27 and 32-33, the number of any other size meteoroid relative to 10^{-3} gram is found. For example, the asteroid flux varies as $m^{-0.84}$ (for $m \geq 10^{-9}$ gram) and the cometary flux varies as $m^{-1.213}$ (for $m \geq 10^{-6}$ gram). Thus to obtain the number of meteoroid impacts per unit area for 10^{-4} gram (an order of magnitude smaller), the 10^{-3} gram fluxes would be increased by the factors $10^{1.213}$ and $10^{0.84}$ for cometary and asteroidal meteoroids, respectively. Thus for m = 10^{-4} gram

$$\frac{N_c}{A} = 10^{1.213} \times 1.71 \times 10^{-4}/m^2 = 2.79 \times 10^{-3}/m^2$$

$$\frac{N_a}{A} = 10^{0.84} \times 2.46 \times 10^{-3}/m^2 = 1.70 \times 10^{-2}/m^2$$

$$\frac{N_t}{A} = 1.98 \times 10^{-2}/m^2$$

The average velocity for particles of 10^{-4} gram and larger would be

$$V_t = \frac{2.79 \times 10^{-3} \times 20.9 + 1.70 \times 10^{-2} \times 15.7}{1.98 \times 10^{-2}} = 16.4 \text{ km/sec.}$$

The probability of not being hit by a meteoroid of mass m or larger is given by

$$P_o = e^{-N_t} \qquad \text{(A16)}$$

Thus, for the sample spacecraft of 10 m^2 of surface area,

$$P_o (m = 10^{-3}) = 0.974$$

$$P_o (m = 10^{-4}) = 0.82$$

If $P_o = 0.974$ is considered an acceptable probability, then the spacecraft surface area should be designed to survive a meteoroid impact of 10^{-3} gram at 16.0 km/sec.

A.2 Simplified Model (Integration Along Trajectory Approximated)

A.2.1 Cometary Flux

The values of the various parameters to be used in the equations in section 3.2.1 are as follows:

$$R_1 = 1.0 \text{ AU}$$

$$R_2 = 5.07 \text{ AU}$$

$$\theta_r(R_1) = 0$$

$$\theta_r(R_2) = 0.76$$

$$t = 5.2 \times 10^7 \text{ sec}$$

so that

$$\log \bar{F}_c = -15.07 - 1.213 \log m$$

or for $m = 10^{-3}$ g,

$$\bar{F}_c = 3.7 \times 10^{-12}/\text{m}^2\text{-sec}$$

or

$$\frac{N_c}{A} = \bar{F}_c t = 1.93 \times 10^{-4}/\text{m}^2$$

The average cometary velocity for the mission is found to be 20 km/sec.

A.2.2 Asteroidal Flux

The total number of asteroidal impacts is given in section 3.2.2 as

$$\frac{N_a}{A} = 10^{-5.0} m^{-0.84}$$

or for m = 10^{-3} gram

$$\frac{N_a}{A} = 3.3 \times 10^{-3}/\text{square meter}$$

The average asteroidal velocity for the mission V_a (R = 2.5) is found to be about 16 km/sec.

APPENDIX B

GLOSSARY

Asteroids – A group of bodies in orbit around the Sun whose orbit usually lies between Mars and Jupiter. Planetary perturbations have caused a few asteroids to be found outside this region. Observed asteroids have diameters ranging from a few kilometers to a few hundred kilometers. An asteroidal meteoroid is a meteoroid originating from larger asteroids.

Comets – A group of bodies, usually in highly elliptical orbits around the Sun. The nucleus of a comet appears to be of low density and to contain solid material as well as volatile gases. A cometary meteoroid is a meteoroid originating from the nucleus of a comet.

Ecliptic Plane – The plane of the Earth's orbit.

Gegenschein – A dim patch of light, several degrees in diameter, seen in the anti-solar direction. The origin of this light is still controversial.

Geometric Albedo – A measure of the fraction of light reflected in the direction of the incident light source.

Heliocentric Latitude and Longitude – Latitude and longitude using the Sun as the center of the coordinate system. The position of the Sun as seen from the Earth at vernal equinox (first day of spring in the northern hemisphere) is the direction of zero longitude, and the ecliptic plane is zero latitude (fig. B.1).

Meteor – The light phenomenon which results from the entry of a meteoroid into the Earth's atmosphere.

Meteorite – A meteoroid which has reached the surface of the Earth without being completely vaporized.

Meteoroid – A solid object moving in interplanetary space, usually in the size range from about 10^{-12} gram or smaller to several grams.

Orbital Elements – See figure B.2.

Zodiacal Light – An elliptical disk of light around the Sun, usually seen just before sunrise, or after sunset. This light is caused by reflected light from meteoroids.

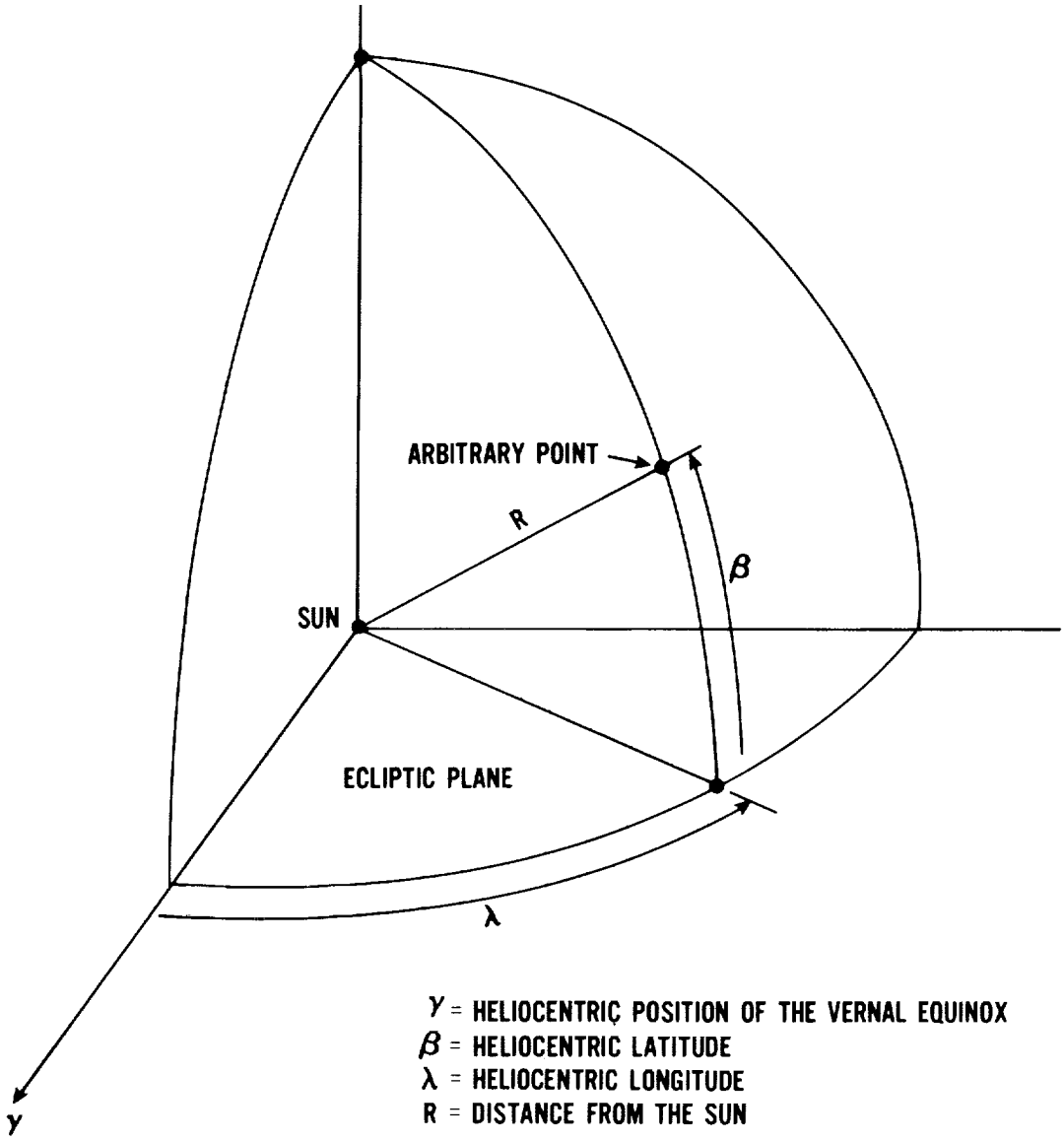

Figure B.1 – Definition of heliocentric latitude and longitude

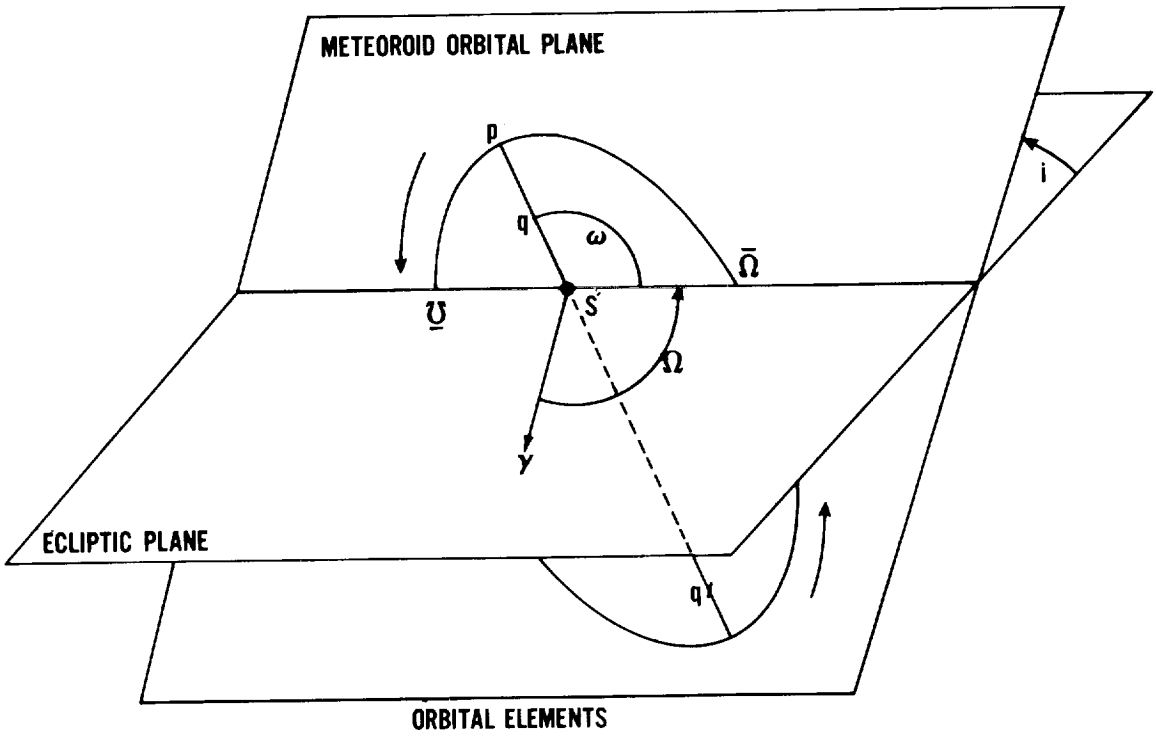

p = POINT OF PERIHELION
q = PERIHELION DISTANCE, ASTRONOMICAL UNITS
q' = APHELION DISTANCE, ASTRONOMICAL UNITS
a = ½ (q + q') = SEMI–MAJOR AXIS, ASTRONOMICAL UNITS

$$e = \frac{q' - q}{q' + q} = \text{ECCENTRICITY}$$

S = SUN
γ = HELIOCENTRIC POSITION OF THE VERNAL EQUINOX
i = INCLINATION OF METEOROID ORBITAL PLANE, DEG
$\bar{\omega} = \Omega + \omega$ = LONGITUDE OF PERIHELION, DEG
Ω = LONGITUDE OF ASCENDING NODE, DEG
Ω̄ = ASCENDING NODE
℧ = DESCENDING NODE
ω = ARGUMENT OF PERIHELION, DEG

Figure B.2 – Definition of orbital elements.

NASA SPACE VEHICLE DESIGN CRITERIA MONOGRAPHS NOW ISSUED

SP-8001	(Structures)	Buffeting During Launch and Exit, May 1964
SP-8002	(Structures)	Flight-Loads Measurements During Launch and Exit, December 1964
SP-8003	(Structures)	Flutter, Buzz, and Divergence, July 1964
SP-8004	(Structures)	Panel Flutter, May 1965
SP-8005	(Environment)	Solar Electromagnetic Radiation, June 1965
SP-8006	(Structures)	Local Steady Aerodynamic Loads During Launch and Exit, May 1965
SP-8007	(Structures)	Buckling of Thin-Walled Circular Cylinders, revised August 1968
SP-8008	(Structures)	Prelaunch Ground Wind Loads, November 1965
SP-8009	(Structures)	Propellent Slosh Loads, August 1968
SP-8010	(Environment)	Models of Mars Atmosphere (1967), May 1968
SP-8011	(Environment)	Models of Venus Atmosphere (1968), December 1968
SP-8012	(Structures)	Natural Vibration Modal Analysis, September 1968
SP-8013	(Environment)	Meteoroid Environment Model - 1969 (Near-Earth to Lunar Surface), March 1969
SP-8014	(Structures)	Entry Thermal Protection, August 1968
SP-8015	(Guidance and Control)	Guidance and Navigation for Entry Vehicles, November 1968
SP-8016	(Guidance and Control)	Effects of Structural Flexibility on Spacecraft Control Systems, April 1969
SP-8017	(Environment)	Magnetic Fields - Earth and Extraterrestrial, March 1969
SP-8018	(Guidance and Control)	Spacecraft Magnetic Torques, March 1969

SP-8019	(Structures)	Buckling of Thin-Walled Truncated Cones, September 1968
SP-8020	(Environment)	Mars Surface Models (1968), May 1969
SP-8021	(Environment)	Models of Earth's Atmosphere (120 to 1000 km), May 1969
SP-8023	(Environment)	Lunar Surface Models, May 1969
SP-8024	(Guidance and Control)	Spacecraft Gravitational Torques, May 1969
SP-8025	(Chemical Propulsion)	Solid Rocket Motor Metal Cases, April 1970
SP-8027	(Guidance and Control)	Spacecraft Radiation Torques, October 1969
SP-8028	(Guidance and Control)	Entry Vehicle Control, November 1969
SP-8029	(Structures)	Aerodynamic and Rocket-Exhaust Heating During Launch and Ascent, May 1969
SP-8031	(Structures)	Slosh Suppression, May 1969
SP-8032	(Structures)	Buckling of Thin-Walled Doubly Curved Shells, August 1969
SP-8034	(Guidance and Control)	Spacecraft Mass Expulsion Torques, December 1969

NASA-Langley, 1971 —— 30